Stem Cell Reports
Article

ISSCR

OPEN ACCESS

Rare intercellular material transfer as a confound to interpreting inner retinal neuronal transplantation following internal limiting membrane disruption

Kevin Y. Zhang,[1,2] Arumugam Nagalingam,[1] Stella Mary,[1] Erika A. Aguzzi,[1] Weifeng Li,[1] Nitin Chetla,[1] Barbara Smith,[3] Michael E. Paulaitis,[4] Malia M. Edwards,[1] Harry A. Quigley,[1] Donald J. Zack,[1,5] and Thomas V. Johnson[1,6,*]

[1]Glaucoma Center for Excellence, Wilmer Eye Institute, Johns Hopkins University School of Medicine, Baltimore, MD, USA
[2]Department of Pathology, Johns Hopkins University School of Medicine, Baltimore, MD, USA
[3]Department of Cell Biology, Johns Hopkins University School of Medicine, Baltimore, MD, USA
[4]Center for Nanomedicine, Wilmer Eye Institute, Johns Hopkins University School of Medicine, Baltimore, MD, USA
[5]Departments of Neuroscience, Molecular Biology and Genetics, and Genetic Medicine, Johns Hopkins University School of Medicine, Baltimore, MD, USA
[6]Cellular and Molecular Medicine Program, Johns Hopkins University School of Medicine, Baltimore, MD, USA
*Correspondence: johnson@jhmi.edu
https://doi.org/10.1016/j.stemcr.2023.09.005

SUMMARY

Intercellular cytoplasmic material transfer (MT) occurs between transplanted and developing photoreceptors and ambiguates cell origin identification in developmental, transdifferentiation, and transplantation experiments. Whether MT is a photoreceptor-specific phenomenon is unclear. Retinal ganglion cell (RGC) replacement, through transdifferentiation or transplantation, holds potential for restoring vision in optic neuropathies. During careful assessment for MT following human stem cell-derived RGC transplantation into mice, we identified RGC xenografts occasionally giving rise to labeling of donor-derived cytoplasmic, nuclear, and mitochondrial proteins within recipient Müller glia. Critically, nuclear organization is distinct between human and murine retinal neurons, which enables unequivocal discrimination of donor from host cells. MT was greatly facilitated by internal limiting membrane disruption, which also augments retinal engraftment following transplantation. Our findings demonstrate that retinal MT is not unique to photoreceptors and challenge the isolated use of species-specific immunofluorescent markers for xenotransplant identification. Assessment for MT is critical when analyzing neuronal replacement interventions.

INTRODUCTION

The mammalian retina and optic nerve possess limited spontaneous regenerative potential (Williams et al., 2020). As a result, optic neuropathic vision loss is irreversible and a major cause of visual morbidity worldwide (Tham et al., 2014). Current therapeutic strategies for optic neuropathies mitigate disease progression by modifying pathologic risk factors (e.g., elevated intraocular pressure in glaucoma) but novel therapies are needed to restore lost vision. Neuronal replacement strategies hold significant potential for reversing blindness from retinal and optic nerve diseases. Indeed, human photoreceptor transplantation has achieved considerable experimental success (Ribeiro et al., 2021; Gasparini et al., 2022) and is nearing clinical trial (Singh et al., 2020). The validity of neuronal transplantation studies relies on cell-tracking methodologies to differentiate donor from host cells for quantification of donor cell survival and engraftment. This is typically achieved with donor-specific transgenic fluorescent reporters (e.g., GFP) (MacLaren et al., 2006; Tucker et al., 2011; Pearson et al., 2012), although immunofluorescent labeling of species-specific antigens has also been employed in xenotransplant settings (Ribeiro et al., 2021; Gasparini et al., 2022).

Initial studies documenting functional visual restoration following photoreceptor transplantation in animal models attributed the outcome to donor cell integration within the degenerating host retina (MacLaren et al., 2006; Pearson et al., 2012; Barber et al., 2013; Singh et al., 2013). However, a substantial body of work subsequently revealed that a large proportion of purportedly integrated donor photoreceptors were actually endogenous cells that had been labeled artifactually, resulting from intercellular transfer of donor-derived cytoplasmic materials including fluorescent proteins (Pearson et al., 2016; Santos-Ferreira et al., 2016; Singh et al., 2016; Decembrini et al., 2017; Ortin-Martinez et al., 2017). This process, termed intercellular material transfer (MT), facilitates host cell acquisition of donor-derived fluorescent markers, nucleic acids, proteins, and organelles. In the search to identify the causative mechanism for MT, several possibilities have emerged, including cell fusion, endocytosis (Generous et al., 2019), and gap junctions (Valiunas et al., 2005). Recent transplantation studies determined that tunneling nanotubes (TNTs), consisting of actin-rich cytoplasmic bridges connecting neighboring cells (Rustom et al., 2004; Yamashita et al., 2018), mediate donor-to-host photoreceptor MT in photoreceptors (Kalargyrou et al., 2021; Ortin-Martinez et al., 2021). Nanotube-mediated horizontal MT also occurs between endogenous photoreceptors during development (Kalargyrou et al., 2021; Heisterkamp et al., 2022). Collectively, these findings have prompted

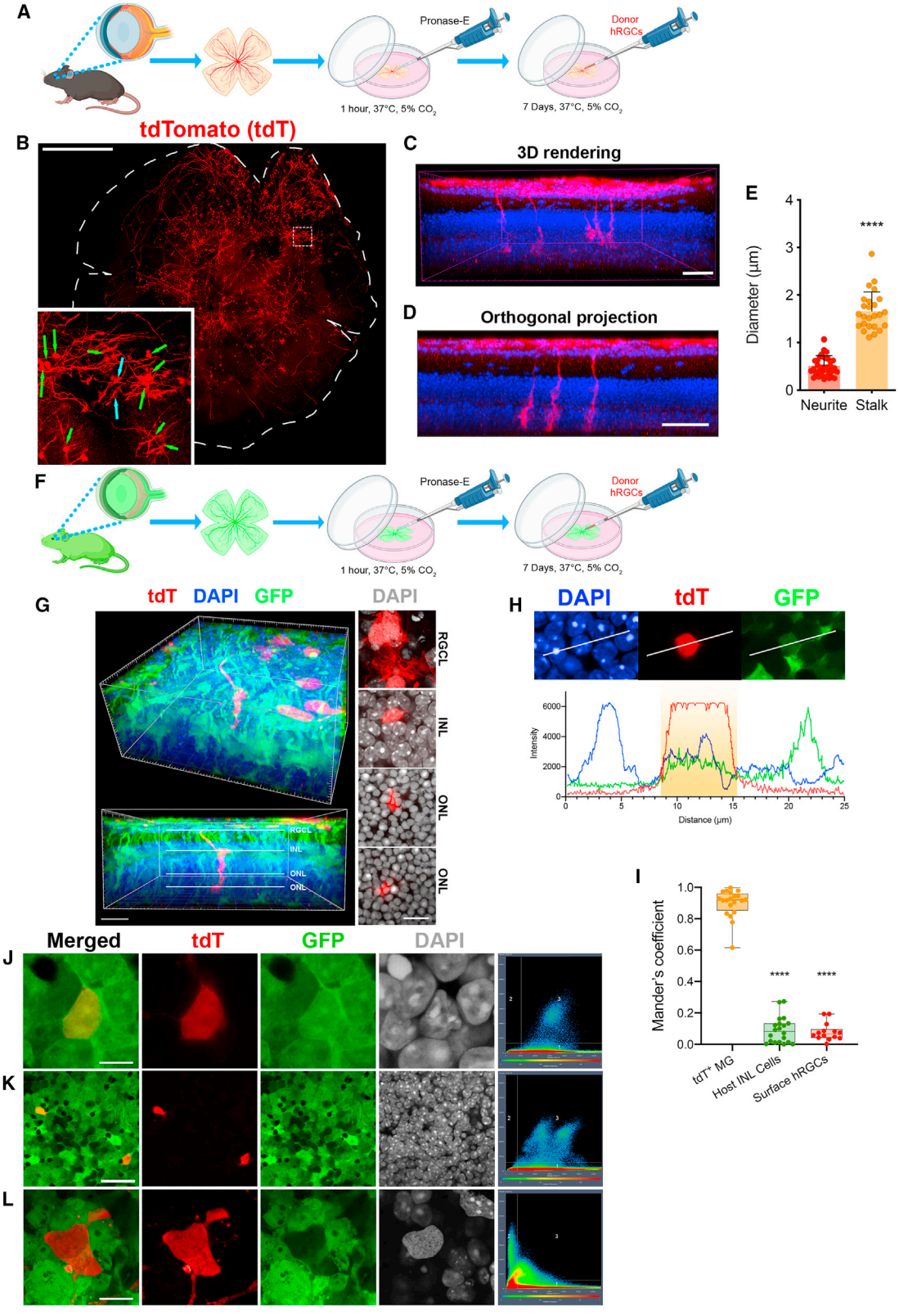

(legend on next page)

stringent reexamination of neuronal transplantation results and raised concerns regarding the fidelity of fluorescent tracking tools (Johnson et al., 2023).

While retinal MT has so far only been reported to take place between photoreceptors, it remains unclear whether the phenomenon might also occur among other retinal cell types. Furthermore, MT necessitates careful analysis and interpretation of cell replacement approaches using a variety of donor sources. Considering these findings, we sought to interrogate whether MT is PR specific by conducting rigorous assessments of donor marker expression in retinal cells following both *ex vivo* and *in vivo* retinal ganglion cell (RGC) transplantation.

RESULTS

tdTomato is transferred from donor human RGCs to host retinal cells following transplantation

We transplanted human embryonic stem cell (hESC)-derived RGCs (hRGCs) onto the inner (vitreous) surface of adult mouse organotypic retinal explants following enzymatic internal limiting membrane (ILM) disruption using the proteolytic enzyme Pronase E (Figure 1A). We previously showed that this approach enhances donor hRGC integration both in organotypic retinal explant cultures (Zhang et al., 2021; Zhang and Johnson, 2022) and *in vivo* (Aguzzi et al., 2022) without inducing discernible neuroretinal cell death but is associated with modest reactive gliosis (Aguzzi et al., 2022). Donor hRGCs expressed red fluorescent tdTomato (tdT) under the control of endogenous *BRN3B* promoter (Sluch et al., 2017), which filled the soma and neurites and enabled tracking and localization of donor neurons post-transplantation. After 7 days of co-culture, integrated hRGC neurites exhibited thin, dendriform, branched processes, which localized primarily to the inner plexiform layer (IPL), but which also occasionally grew into the inner nuclear layer (INL) or deeper, as described previously (Zhang et al., 2021). In addition, we observed tdT expression in cells that was less intense than in hRGCs and which did not conform to a typical neuronal morphology (Figures 1B–1D). 3D reconstructions of tiled confocal retinal flatmounts demonstrated that these atypical tdT$^+$ cells formed thick radial processes extending in the apico-basal orientation from the vitreoretinal interface to beyond the outer nuclear layer (ONL) (Figures 1C and 1D). These processes were linear with few short branches and diameters significantly greater than those of integrated donor hRGC neurites (Figure 1E; hRGC neurite diameter: 0.51 ± 0.21 μm; atypical tdT$^+$ radial process diameter: 1.66 ± 0.41 μm; $p < 0.0001$). Each atypical tdT$^+$ cell contained a single nucleus within the INL. The distal termini of their processes formed footplates overlying neurons in the RGCL as well as interdigitations surrounding photoreceptors in the ONL (Video S1). Their unique cellular anatomy morphologically resembled Müller glia (MG) (Reichenbach and Bringmann, 2020).

A more definitive method for discriminating host and recipient cells involves transplanting tdT$^+$ hRGCs into a transgenic host expressing a second traceable marker, to assess for mutual exclusivity of reporter proteins in corresponding lineages (Pearson et al., 2016; Singh et al., 2016). Therefore, we transplanted hRGCs onto retinal explants derived from C57BL/6-Tj(CAG-EGFP)1Osb/J mice that express GFP ubiquitously (Figure 1F) (Okabe et al.,

Figure 1. Characteristics of atypical tdT-expressing cells in the host retina

(A) Schematic describing hRGC co-culture on murine organotypic retinal explants with ILM disruption by Pronase E.

(B) En face view of a Pronase E pre-treated organotypic retinal explant at 7 days following tdT$^+$ hRGC co-culture, imaged in flatmount. Dashed lines denote the explant boundary. The inset corresponds to the magnified view of the white-dashed square; green arrows point to typical hRGCs and cyan arrows point to atypical tdT$^+$ cells.

(C and D) Magnified confocal 3D rendering (C) and orthogonal projection (D) of atypical tdT$^+$ cells in the host retina.

(E) Measured diameters of individual neurites elaborated from donor hRGCs (n = 40 cells from 5 retinas) compared with the diameters of radial processes in the atypical tdT$^+$ cells (n = 25 cells from 5 retinas).

(F) Schematic describing hRGC co-culture on Pronase E pre-treated GFP-expressing host retinal explants.

(G) 3D rendering and orthogonal projection of tdT$^+$ retinal cells in GFP-expressing host retina. DAPI stained all nuclei (blue). The panels on the right depict orthogonal z slices at the retinal layers indicated by the white lines in the profile view; tdT (red) labeling in atypical cells spanned all retinal layers as shown by DAPI (white).

(H) Fluorescence intensity histogram showing overlapping peaks (yellow highlight) of tdT and GFP fluorescence when sampled through the cytoplasm of an atypical tdT$^+$ cell in the GFP$^+$ recipient retinal INL.

(I) Box and whiskers plots of Mander's coefficient for tdT and GFP fluorescence from atypical tdT$^+$ cells (n = 20 cells from 9 retinas), tdT$^-$ GFP$^+$ host cells (n = 20 cells from 2 retinas), and tdT$^+$ hRGCs (n = 14 cells from 2 retinas).

(J and K) Single z slices of confocal stacks show that GFP and tdT were co-expressed in the soma of atypical tdT$^+$ cells in the INL. Scatterplots of GFP (x axis) and tdT (y axis) fluorescent intensity demonstrate high degrees of co-localization.

(L) tdT$^+$ hRGCs near the host RGCL did not express GFP. Scale bars, 1 mm (B), 30 μm (C, D, G, and K), 20 μm (G), 10 μm (z slices of G and L), and 5 μm (J). Data are represented as mean ± SD.

1997). Following a 7-day co-culture period, 100% of the sampled atypical tdT$^+$ cells (n = 68 from 11 retinas) were also GFP$^+$, suggesting an endogenous host origin (Figures 1G–1K; Video S2). Scatterplots of tdT and GFP fluorescent intensities within confocal z slices showed distinct overlap in these presumed endogenous tdT$^+$ cells (Figures 1J and 1K), which was confirmed by examining fluorescent intensity histograms of GFP and tdT fluorescence through the cell somata (Figure 1H). Notably, tdT$^+$ integrated hRGCs located within the RGCL and more superficial non-integrated hRGCs were uniformly GFP$^-$ (Figure 1L), suggesting that transfer of host-derived GFP to donor hRGCs in the inner retina does not occur.

We quantitatively analyzed the co-localization of donor and host cytoplasmic markers by computing the Manders' overlap coefficient (MOC) (Manders et al., 1992) in the atypical tdT$^+$ recipient cells, the surrounding INL host cells, and donor hRGCs in the RGCL (Figure 1I). We calculated an average MOC of 0.90 ± 0.09 in tdT recipients in the INL (n = 20 cells in 6 transplanted retinas) indicating strong co-expression of tdT and GFP, which was significantly higher than that of host INL cells or donor hRGCs (0.09 ± 0.08 and 0.08 ± 0.06, respectively; $p < 0.0001$). Together, these results suggest transfer of cytoplasmic fluorescent marker occurred unidirectionally from the donor hRGCs to apparently host-derived retinal cells. Notably, co-expression of host-derived GFP in the atypical tdT$^+$ cells indicate they are unlikely to have been the result of tdT$^+$ donor cell transdifferentiation into an MG-like phenotype, unless the phenomenon was also accompanied by host-to-donor GFP MT and adoption of a remarkable degree of structural and morphologic similarity to host MG.

Atypical tdT$^+$ cells receptive of MT are MG

We next investigated the cellular identity of the atypical tdT$^+$ cells. Given their morphologic similarity to MG, we immunolabeled transplanted retinal explants with antibodies against the glial-specific intermediate filaments glial fibrillary acid protein (GFAP), vimentin, and nestin. Following stressful conditions, such as explantation or intravitreal injection, intermediate filament expression typically increases as a feature of reactive gliosis. GFAP was strongly expressed in retinal nerve fiber layer astrocytes and in MG (Figures 2A and 2D). Using 3D renderings of confocal z stacks of retinal flatmounts (Figure 2D) or retinal cryosections (Figure 2A), we observed strong co-localization of tdT and GFAP in all tdT$^+$ host retinal cells, whereas GFAP did not co-localize with tdT$^+$ hRGCs in the inner retina. Vimentin co-localized with tdT$^+$ host retinal cell processes that extended radially from the ILM to the OLM (Figure 2B). Although expression of nestin was comparatively lower in cultured retinal explants, immunoreactivity was detectable in radial glial fibers, which co-localized with tdT$^+$ in host retinal cells (Figure 2C). Whether glial activation is a prerequisite or a consequence of MT is unclear.

To further confirm the identity of cells recipient of tdT MT, we compared the somal position of host tdT$^+$ cells with endogenous MG, rod bipolar cells, and GABAergic amacrine cells in adult mouse retinas immunolabeled with glutamine synthetase (GS), protein kinase C α (PKCα), and glutamic acid decarboxylase 67 (GAD67), respectively. Each cell type has a soma resident in the INL at a distinct positional depth distribution. MG somas predominate centrally within the INL, separating the outer bipolar and horizontal cells from the inner amacrine cells (Jeon et al., 1998). In our positional analysis, PKCα$^+$ rod bipolar cell bodies mostly resided in the outer third of the INL, whereas GAD67$^+$ amacrine cells resided predominantly in the inner third of the INL. GS$^+$ MG distribution peaked in the middle third of the INL, which matched tdT$^+$ host retinal cell soma localization (Figure 2G).

To assess for the possibility that our donor hRGCs may have included a minor population of contaminating donor-derived MG, we conducted multiple additional analyses. First we performed single-cell RNA sequencing on freshly purified pre-transplant purified hRGCs. Comparison with a reference dataset obtained from human fetal retina (Hu et al., 2019) using Seurat label transfer demonstrated that our hRGCs contained major cell populations similar to human fetal RGCs, as well as minor populations that resembled horizontal cells, photoreceptors, retinal progenitor cells, and retinal pigment epithelium (Figure S1A). We did not detect any cells resembling MG. Our purified donor neurons expressed canonical RGC-specific genes including *ATOH7*, *POU4F2*, *ISL1*, and *SNCG* (Figure S1B), but none expressed detectable levels of the MG-specific genes *AQP4*, *CAV*, *CLU*, *GFAP*, *KIR4.1*, or *2.1*, *PRSS2*, *RLPB1*, *S100A16*, *SPBC25*, *EBE1C*, *BING3*, or *CRLBP1* (Figure S1B). Very few cells expressed low levels of MG-associated genes *APOE*, *GNAI2*, *GPR37*, *LHX2*, and *SOX2*, although some cells demonstrated persistent expression of genes shared by retinal progenitor cells, including *CLU*, *DBI*, *DKK3*, *NES*, and *VIM*, which likely indicates an immature state of differentiation (Figure S1B). How cryopreservation and thawing of banked hRGCs changes their transcriptomic phenotype remains to be determined.

Next, we performed immunofluorescent labeling of cultured cells to compare protein expression patterns in purified, pre-transplant, cryopreserved, and then thawed hRGCs, undifferentiated hESCs, human 293T cells, and an immortalized human MG cell line (MIO-M1) (Figure S1C). To determine whether our purified RGCs contained a minor population of proliferating progenitor cells, we assessed Ki67 immunoreactivity. Although 100% of hESCs, 293T cells, and MG were proliferative and expressed

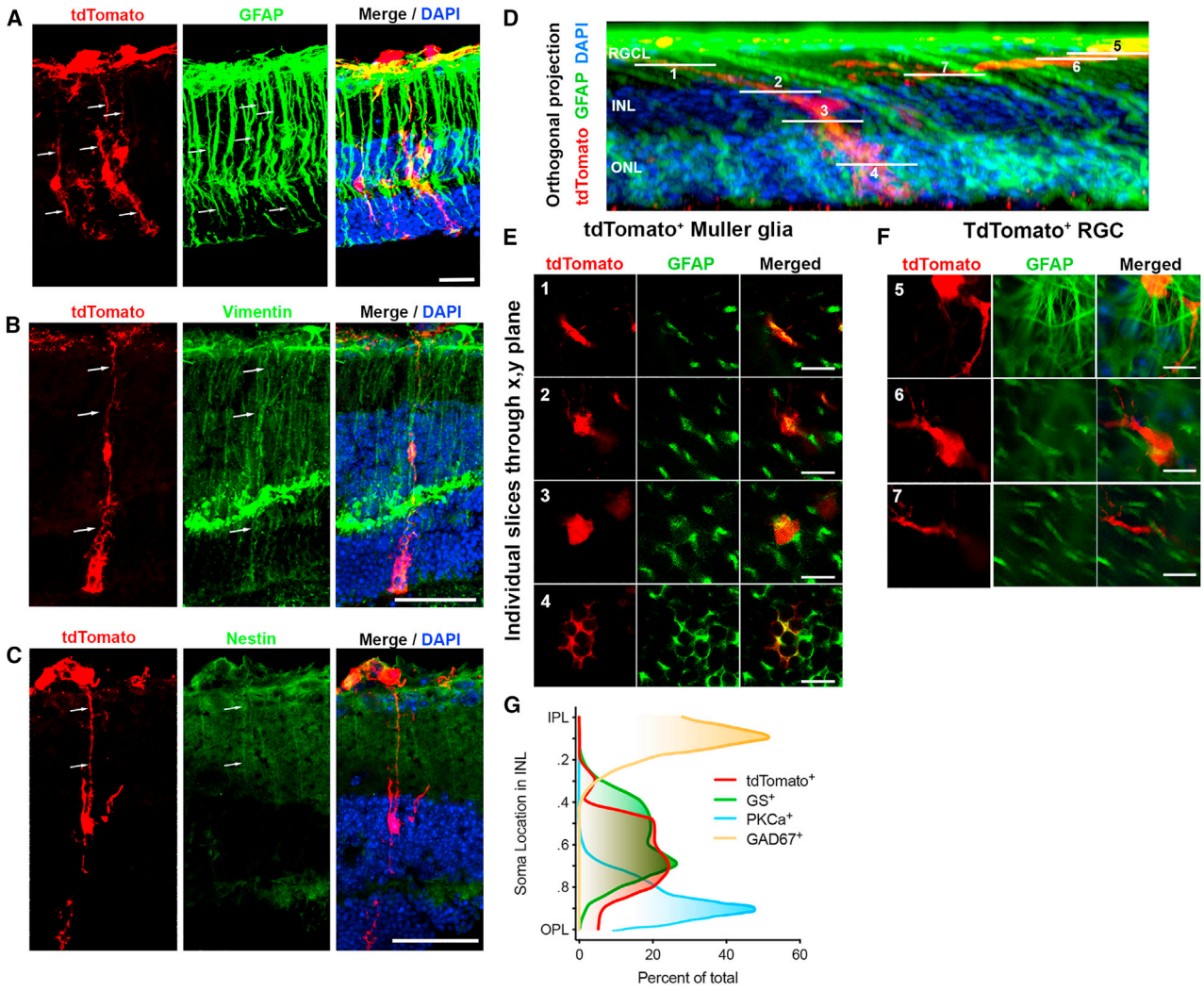

Figure 2. Host tdT⁺ cells are Müller glia

Pronase E pre-treated retinal explants co-cultured with tdT⁺ hRGCs for 7 days exhibited tdT expression in radially oriented cells. Cryosections (A–C) demonstrated co-localization of tdT⁺ host retinal cells with GFAP (A), vimentin (B), and nestin (C). Retinal explants were imaged in flatmount configuration using confocal microscopy and orthogonal projection (D) or individual z slices (E and F) are shown, which demonstrate co-localization between tdT⁺ host cells and GFAP (D and E), but not tdT⁺ hRGCs near the RGCL or their dendrites in the IPL (D and F). Distributions of somal localization within the INL from major cell types in that retinal layer, defined as the proportion of cell bodies at various depths in the INL area plotted as a histogram (G) (tdT⁺ cells: n = 20 cells from 9 retinas; GS, PKCα, and GAD67: n = 40 cells from 2 retinas). Scale bars, 50 μm (A–C) and 10 μm (E and F).

Ki67⁺, we identified no hRGCs that expressed Ki67 (n = 200 cells evaluated per cell type). We evaluated the neuronal phenotype of hRGCs and found that they expressed MAP2 (100% of n = 100 cells), Tau (100% of n = 50 cells), and Brn3b (96% of n = 50 cells), whereas no hESCs, 293T, or MG cells expressed these markers. We also evaluated the glial or progenitor phenotype of our cell cultures and found that Sox2 was expressed by 79% of hESCs (n = 100 cells) and 57% (n = 160 cells) of MG, GFAP was expressed by 22% (n = 200 cells) of MG, GS was expressed by 100% (n = 200 cells) of MG, and vimentin was expressed by 100% (n = 200 cells) of MG. However, none of these markers were expressed by hRGCs (n = 100 cells, Figure S1C). Therefore, while our donor hRGCs may have contained minor populations of cells with a non-RGC transcriptomic signature, they uniformly expressed neuronal markers and we detected no contaminating MG and no proliferating cells.

In sum, our morphological, biochemical, and localization data are all consistent with the host retinal cells recipient of tdT being endogenous MG, and that the donor source of the material is most likely hRGCs, although

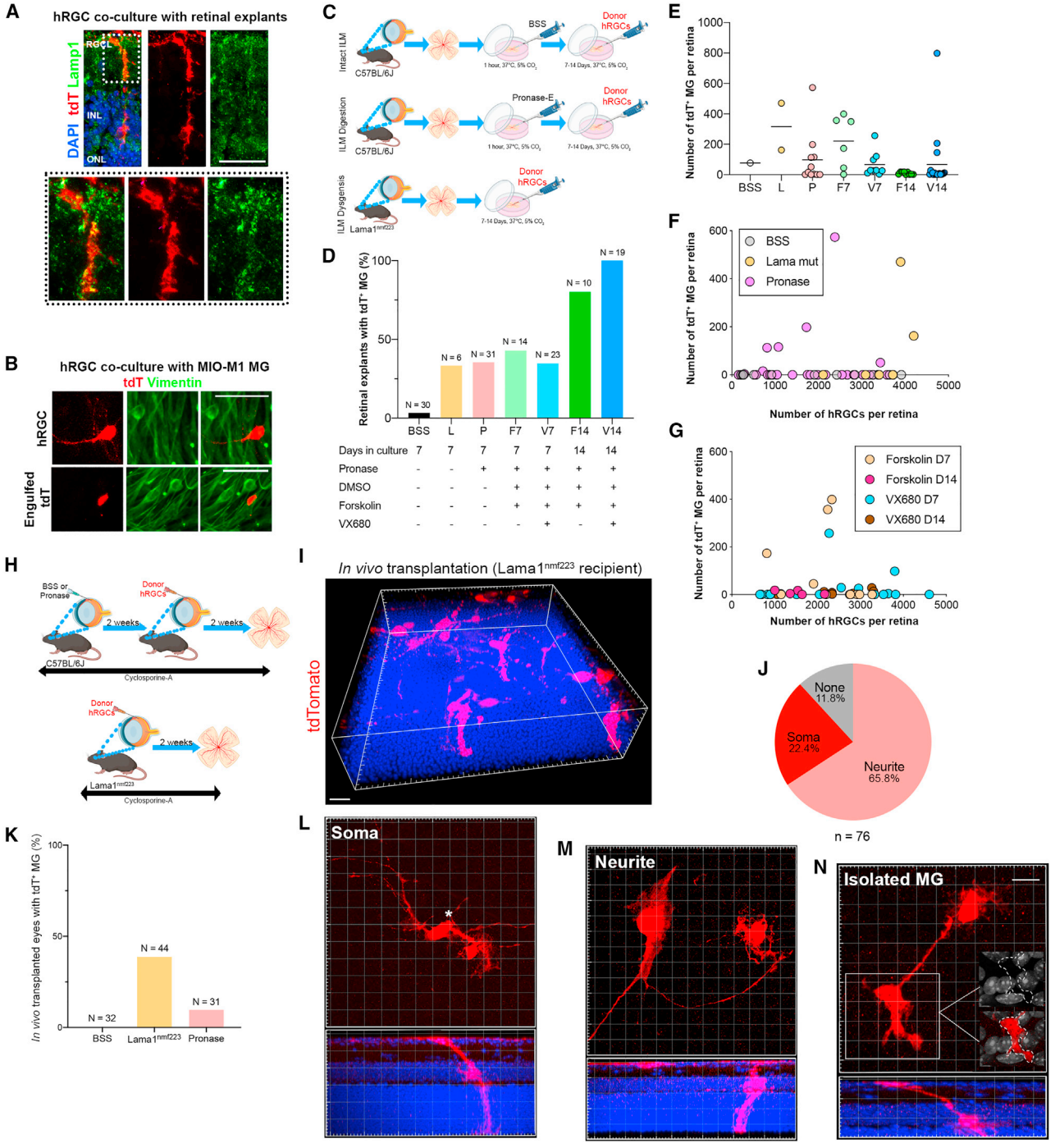

Figure 3. Material transfer from hRGCs to Müller glia requires ILM disruption and is contact dependent in retinal explant cultures and following transplantation *in vivo*

(A) Immunolabeled retinal explant cryosection showing punctate Lamp1 expression (green) within a tdT$^+$ MG stalk (red). The tdT fluorescence extends beyond Lamp1$^+$ puncta.

(B) Epifluorescent microscopy of hRGCs and MIO-M1 MG in co-culture after 5 days. Homogeneous tdT expression in hRGCs and their neurites did not co-localize with vimentin (green; top row). Punctate tdT$^+$ debris was confined inside an MG soma as labeled by vimentin (bottom row).

(C) Experimental design for hRGC co-cultures with retinal explants with or without ILM disruption.

(legend continued on next page)

contaminant populations of differentiating progenitor cells cannot be ruled out as a potential source of these rare events

No evidence for MT to MG occurring through phagocytosis or extracellular vesicles

Although the uniform intensity and complete cytosolic pattern of tdT fluorescence within host MG argued against phagocytic uptake of fluorescent protein as a primary mechanism of reporter acquisition (Sakami et al., 2019), we immunolabeled retinal cryosections for Lamp1 to determine the extent to which intracellular tdT was compartmentalized in phagolysosomes. Confocal microscopy demonstrated the presence of phagolysosome vesicles throughout the host retina (Figure 3A). Although Lamp1 was expressed in the tdT^+ MG stalk, tdT labeling was more extensive and not confined to the Lamp1 puncta, suggesting that the fluorescent marker was primarily cytoplasmic and not intravesicular.

To further evaluate differences in the appearance of cytoplasmic versus phagocytosed tdT in retinal cells, we co-cultured hRGCs with immortalized human MG (from the MIO-M1 cell line) (Limb et al., 2002). After 5 days in culture, all sampled tdT^+ cells in culture were hRGCs and not MG, based on their neuronal morphology and lack of vimentin expression (n = 500 cells, Figure 3B). However, we did identify clumped, amorphous tdT^+ material inside some MG that did not fill the entire cytoplasm, suggesting that MG had phagocytosed debris from dying hRGCs (Figure 3B). Notably, the discrete compartmentalization of tdT signal inside MG was in clear contrast to the uniform pan-cytoplasmic tdT labeling of mouse MG in retinal tissue *in situ* and inconsistent with mere phagocytosis of fluorescent protein from dead hRGCs in living retinas.

Even though PRs appear to engage in MT through TNT communication, we next sought to determine whether extracellular vesicles (EVs) might be carriers of hRGC donor material. EVs are membrane-bound vesicles released into the extracellular space that have been shown to transport cargos including nucleic acids, proteins, and organelles (Budnik et al., 2016). We performed ultracentrifugation on conditioned hRGC culture medium to obtain EV isolates. We then conducted microfluidic resistive pulse sensing to assess the particle size distribution and number concentration, and single-particle interferometric reflectance imaging with fluorescence detection using ExoView Tetraspanin kits to screen for common tetraspanin EV biomarkers. Finally, we visualized the EVs by transmission electron microscopy. These results were consistent with known parameters of EVs (Figures S2A–S2D) (Arab et al., 2021). We then administered purified hRGC-derived EVs to organotypic retinal explant cultures following ILM disruption but without hRGC co-culture, and failed to recapitulate tdT^+ expression in host MG (n = 8 retinas). Although *tdT*, *RBPMS*, and *TUBB3* were detectable in EVs, their expression levels were orders of magnitude lower than in hRGCs (Figure S2E). These results do not support a hypothesis that hRGC-derived EVs are vehicles for RGC-to-MG MT. However, these results also do not definitively rule out the possibility since inadequate dosing, poor localization of epiretinally applied EVs to the retina, or changes in the phenotype of EVs secreted from cultured RGCs compared with transplanted RGCs could have contributed to these observations.

ILM disruption promotes tdT MT to host MG

To determine whether certain microenvironmental conditions promote tdT expression in host MG, we transplanted hRGCs onto retinal explants cultured under various conditions and for variable durations, and then quantified the prevalence of tdT^+ MG in the host retina. We found that tdT expression in MG occurred almost exclusively in

(D) Prevalence of tdT^+ MG in various explant culture conditions. BSS, balanced salt solution; L, $Lama1^{nmf223}$; P, Pronase E; F7, forskolin-enriched 7-day culture; V7, VX680 (tozasertib)-enriched 7-day culture; F14, forskolin-enriched 14-day culture; V14, VX680-enriched 14-day culture. Refer to figure for sample sizes.
(E) Numbers of tdT^+ MG on explants with at least one tdT^+ MG cell (BSS, n = 1 retina; L, n = 2; P, n = 11; F7, n = 6; V7, n = 9; F14, n = 8; V14, n = 19); explants without any tdT^+ MG were excluded. Horizontal bars indicate group means.
(F and G) Scatterplots demonstrating a lack of correlation between the number of surviving hRGCs (x axis) and the number of tdT^+ MG (y axis) on the same retinal explant (refer to D for sample sizes).
(H) Experimental design for *in vivo* hRGC transplantation experiments.
(I) 3D confocal rendering of an *in vivo* $Lama1^{nmf223}$ recipient retina in oblique view. DAPI stained all nuclei (blue).
(J) Spatial relationships between tdT^+ MG and nearby hRGCs. "Neurite" and "Soma" indicate physical contact between a tdT^+ MG and the respective portion of an hRGC. n = 76 MG from 10 retinas.
(K) Prevalence of atypical tdT^+ cells in various *in vivo* transplantation models.
(L–N) Top images: en face maximum intensity projections of confocal z stacks demonstrating tdT^+ MG and a neighboring hRGC (except in N). Bottom images: corresponding orthogonal profile of confocal z stacks illustrating tdT^+ signal in relation to the retinal layers.
(L) An MG footplate contacting an hRGC soma (asterisk). The hRGC emanates neurites from its soma.
(M) An MG footplate contacting a neurite (asterisk) that is extended from a nearby hRGC.
(N) An MG terminating near over the RGCL as a footplate that is anuclear (inset; DAPI is shown in gray). Scale bars, 20 μm.

recipient retinas with disrupted ILM, which was achieved either by enzymatic ILM digestion using Pronase E (Zhang et al., 2021) or by transplanting (without pronase pre-treatment) onto Lama1^{nmf223} mouse retinas that harbor developmental ILM defects (Edwards et al., 2010; Edwards et al., 2011) compared with BSS-treated retinas with intact ILM (Figure 3C). Although we identified high variability in the number of tdT$^+$ MG per retina (Figure 3E), extending *ex vivo* co-cultures from 7 to 14 days increased the proportion of retinas with tdT$^+$ host MG (Figure 3D), whereas treatment with the neuroprotective kinase inhibitor tozasertib (VX680) (Welsbie et al., 2013) did not consistently increase the prevalence of tdT$^+$ MG (Figures 3D and 3E). Moreover, we did not identify a correlation between the number of surviving hRGCs and the number of tdT$^+$ host MG in retinal explants with disrupted ILM cultured under standard conditions (Figure 3F) or when supplemented with tozasertib (Figure 3G). Thus, ILM disruption dramatically increases the likelihood of tdT MT to host MG in the murine host retina and the prevalence of tdT expression in MG increases over time. Given that ILM disruption also significantly increases the migration of hRGC somas into the retinal parenchyma and the elaboration of dendrites into the IPL (Zhang et al., 2021; Aguzzi et al., 2022), we speculate that the mechanism driving hRGC-to-MG MT involves intercellular contact, akin to the development of TNTs previously described to mediate MT between photoreceptors. Alternatively, ILM disruption may induce other (as yet unidentified) cellular changes to the host retina that promote hRGC-to-MG MT.

MT from donor hRGCs to host MG occurs *in vivo*

To determine whether atypical tdT expression following RGC transplantation might be an artifact or epiphenomenon specific to *ex vivo* retinal explant culture conditions, we analyzed retinal flatmounts 2 weeks after intravitreal injection of donor hRGCs in living, immunosuppressed mice. Recipient mice had intact ILM (C57BL/6J mice pre-treated with intravitreal BSS), digested ILM (C57BL/6J mice pre-treated with intravitreal Pronase E), or dysgenic ILM (as occurs in Lama1^{nmf223} mice) (Figure 3H). Similar to our observations in retinal explants, we identified tdT$^+$ host MG *in vivo* (Figure 3I), and exclusively in retinas with ILM disruption but not in control mice with intact ILM (Figure 3K). Following *in vivo* transplantation of tdT$^+$ hRGCs into mouse eyes with compromised ILM, we identified 76 tdT$^+$ MG in 20 eyes (0 of 32 BSS control eyes; 3 of 31 Pronase E-treated eyes; 17 of 44 Lama1^{nmf223} eyes). In agreement with our hypothesis that hRGC-to-MG MT is mediated by a cell contact-based mechanism, we observed a high degree of apparent continuity in tdT labeling from adjacent hRGCs to the footplates of tdT$^+$ MG. We assessed the spatial association between tdT$^+$ MG and nearby hRGCs, and categorized interactions into one of three types (Figure 3J). In 22.4% of the instances, tdT$^+$ MG footplates were in very close proximity to an overlying hRGC soma (Figure 3L, i.e., with the limits of resolution of confocal microscopy, there was no discontinuity in tdT signal between hRGC and MG detectable), while 65.8% were in close proximity to hRGC neurites (Figure 3M). The remaining 11.8% of the cases involved "isolated" tdT$^+$ MG (Figure 3N), as defined by the absence of hRGCs within a 100 μm radius. We further confirmed that, in the isolated cases, tdT expression near the ILM was not associated with a nucleus, confirming that it came from the terminating footplate of an MG whose soma resided in the INL, and not a transplanted hRGC (Figure 3N). Of note, performing this analysis was only feasible with a sparse density of surviving hRGCs, as is the case following *in vivo* transplantation (Venugopalan et al., 2016; Oswald et al., 2021; Aguzzi et al., 2022; Vrathasha et al., 2022), and thus could not be performed for our *ex vivo* cultures, where a high density of overlapping RGC neurites precluded definitive identification of cell contact between specific cells. The high degree of close proximity between tdT$^+$ MG and hRGCs is consistent with a physical interaction being necessary for tdT expression in host MG. However, the nature of such interactions will require further evaluation using super-resolution or electron microscopy. On the other hand, the occasional presence of tdT expression in "isolated" MG either suggests either that (1) sustained contact with hRGCs is not required and tdT expression in MG may persist for some period of time in host retinal cells after donor hRGCs have migrated away from MT-receptive MG or died, or (2) proximity increases the likelihood of MT but cell contact is not strictly necessary for hRGC-to-MG MT.

To determine whether RGC-to-MG tdT MT might be a phenomenon specific to hRGCs derived from H7 hESCs, we analyzed murine retinas following *in vivo* transplantation of hRGCs differentiated from an independent line of H9 hESCs. We identified a total of 40 tdT$^+$ MG in 49 eyes (8 of 27 Pronase-E-treated eyes; 7 of 22 Lama1^{nmf223} eyes). Similar to results following H7 RGC transplantation, we identified no tdT$^+$ MG following transplantation into eyes with intact ILM. Therefore, hRGC-to-MG MT, and its association with ILM disruption, is not a cell line-specific property.

hSC-derived RGCs and host mouse retinal cells exhibit distinct nuclear morphology

Unambiguously distinguishing donor versus host origin is essential to parsing bona fide engraftment from MT. In an effort to distinguish donor from host cells in our human-to-mouse xenograph paradigm independent of tdT expression, we noted that the nuclear morphologies of mouse

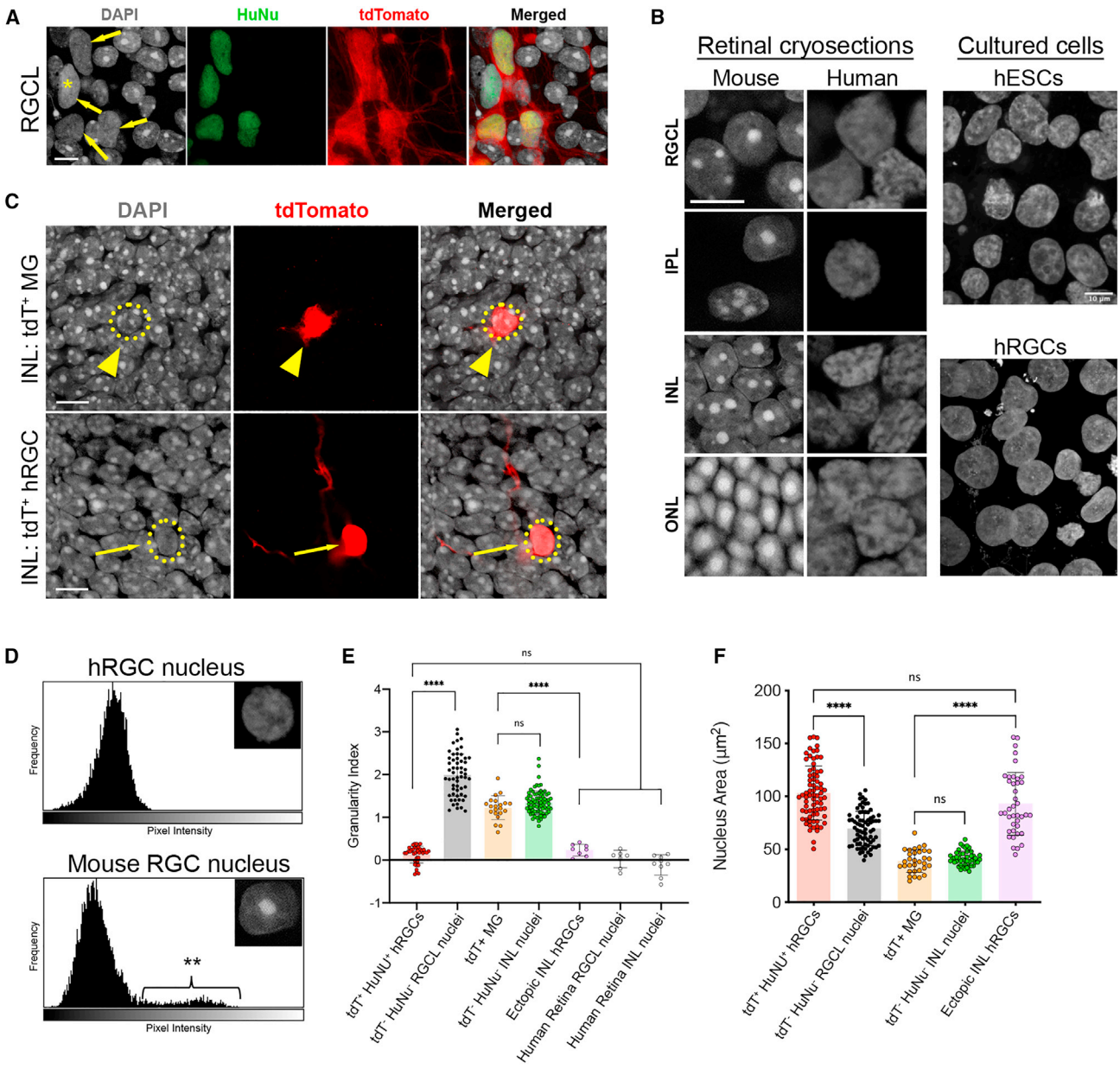

Figure 4. Mouse and human retinal nuclei exhibit distinct nuclear features

(A) Magnified confocal images of a post-transplantation Lama1^{nmf223} retinal explant showing donor hRGCs coplanar with host RGCL cells. tdT$^+$ (red) cells are all HuNu$^+$ (green) and exhibit homogeneous DAPI (gray) staining. In contrast, all tdT$^-$ HuNu$^-$ nuclei in the RGCL have prominent nucleoli. In rare cases, HuNu$^+$tdT$^-$ (asterisk) cells can be observed representing human ESC-derived cells that are BRN3B$^-$.

(B) Confocal images of DAPI (gray)-stained mouse and human retinal sections, and cultured hESCs and hRGCs. Mouse nuclei in all retinal layers revealed distinct nucleoli, whereas human nuclei in all retinal layers did not feature prominent nucleoli.

(C) Confocal slices through the level of tdT$^+$ (red) nuclei in the INL of Lama1^{nmf223} retinal explants. Upper panel shows an example of an tdT$^+$ MG with a heterochromatic nucleus (arrowhead). Lower panel shows an example of an ectopic tdT$^+$ hRGC in the INL with neurite extensions. Dashed lines outline nucleus boundaries.

(D) Representative hRGC and mouse RGCL nuclei with their corresponding DAPI intensity histograms. Mouse RGCL nuclei exhibit a rightward shoulder in the distribution (**).

(E) Quantification of nuclear GI sampled from various retinal layers in mouse and human retinas. tdT$^+$HuNu$^+$ hRGCs, n = 40 cells from 9 retinas; tdT$^-$HuNu$^-$ mRGCs, n = 57 cells from 9 retinas; tdT$^+$ MG, n = 20 cells from 9 retinas; tdT$^-$HuNu$^-$ INL mouse neurons, n = 78 cells from

(legend continued on next page)

and human retinal cells as revealed by DAPI staining are distinct. Near the inner surface retinal explants co-cultured with hRGCs, where donor hRGCs and host RGCL neurons comingle, we observed prominent nucleoli exclusively within the nuclei of host retinal neurons, which were not labeled by a human-specific nuclear antigen antibody (HuNu). In contrast, $HuNu^+$ tdT^+ donor cells demonstrated homogeneous DAPI staining without prominent nucleoli (Figure 4A).

We asked whether this difference in DAPI-visualized nuclear architecture was a general feature of mouse versus human retinal cells, and separately stained cryosections obtained from mouse and postmortem human retinas with DAPI (Figure 4B). Human retinal neurons in all retina layers exhibited bland nuclear architecture without prominent DAPI-bright nucleoli, whereas mouse retinal neurons in the INL and RGCL showed speckled heterochromatic nuclear regions and photoreceptors uniformly exhibited a single central nuclear density. Nuclei of cultured hESCs and differentiated hRGCs revealed morphologies similar to those observed in the postmortem human retinas and in our transplanted donor RGCs (Figure 4B).

When we examined the architecture of tdT^+ MG nuclei in the INL of retinal explants or retinas following *in vivo* transplantation using confocal microscopy, we observed a heterochromatic DAPI nuclear morphology similar to that of the adjacent host mouse neurons (Figure 4C, arrowhead). In contrast, rare hRGCs that had migrated ectopically into the IPL or INL maintained a euchromatic DAPI nuclear morphology distinct from surrounding mouse neurons (Figure 4C, arrow). These integrated hRGCs elaborated lateral neurite growth from their soma and maintained a neuronal morphology distinct from the MG morphology of host-derived tdT^+ cells.

To empirically quantify the observed difference in DNA compaction between mouse recipient and human donor cells in cultured retinal explants, we measured the DAPI pixel intensity distribution of individual nuclei (Figure 4D) and then calculated the skewness of the intensity distribution for each nucleus. We termed this value the granularity index (GI) (Figure 4E). Euchromatic nuclear architecture (as seen in hRGCs) exhibited DAPI pixel intensities with a Gaussian distribution and a skewness near 0. In contrast, prominent nucleoli (as seen in mouse retinal cells) exhibit high DAPI pixel intensities relative to the rest of the nucleus, which cause a positive skew in the DAPI pixel intensity distribution and a positive GI (Figure 4D). We sampled nuclei from $HuNu^+tdT^+$ hRGCs and $HuNu^-tdT^-$ host neurons in the RGCL and found average GI values of 0.13 ± 0.20 and 1.91 ± 0.49, respectively ($p < 0.0001$, Figure 4E), which consistently differentiated the donor or host origin of cells in this retinal layer. Endogenous nuclei sampled from the RGCL and INL of human retinas revealed no significant difference in GI compared with transplanted donor hRGCs (human RGCL: 0.03 ± 0.20; human INL: −0.11 ± 0.24).The average GI of hRGCs that had migrated deeper into the retinal parenchyma (ectopic INL hRGCs) was 0.24 ± 0.14, significantly lower than that of tdT^+ MG in the INL (1.22 ± 0.28; $p < 0.0001$). There was no significant difference in GI between the tdT^+ MG and $HuNu^-tdT^-$ mouse nuclei in the INL (1.35 ± 0.27; $p = 0.07$). In sum, the GI of cells seemingly of human origin (TdT^+ hRGCs irrespective of localization in the retina and retinal cells from postmortem eyes) was near zero, whereas the GI of cells presumably of mouse origin (including tdT^+ MG) were well above 1.

In addition to characterizing nucleolar morphology, we measured the cross-sectional area of host nuclei (Figure 4E). $HuNu^+tdT^+$ hRGCs on the inner retinal surface had an average nuclear cross-sectional area of 103.2 ± 25.4 μm^2, whereas host neurons in the RGCL had a smaller average nuclear cross-sectional area of 69.8 ± 16.2 μm^2 ($p < 0.0001$). There was no significant difference in nuclear area between the tdT^+ MG and the surrounding tdT^- INL host retinal cells (38.9 ± 10.6 and 41.5 ± 6.9 μm^2, respectively; $p = 0.20$). Ectopically migrating $HuNu^+tdT^+$ hRGCs in the INL had significantly larger nuclear areas than host INL neurons (93.0 ± 29.6 μm^2; $p < 0.0001$) but did not significantly differ from that of non-integrated donor hRGCs on the retinal surface.

Our analyses suggest that nuclear architecture and nuclear size are intrinsic properties that can be utilized to distinguish human-derived donor cells from mouse neurons in the host retina following transplantation. MG recipient of tdT MT have nuclei that most closely resemble mouse retinal nuclei, consistent with their presumed host origin.

MT involves multiple donor cell-derived markers

Identifying the specific cargo that is exchanged by retinal cells during hRGC-to-MG MT was inherently challenging due to the relatively low rates of MT and donor hRGC survival compared with those following PR transplantations. Nonetheless, the ability to track human-specific protein

9 retinas; ectopic INL hRGCs, n = 8 nuclei from 9 retinas; human RGCL cells, n = 7 cells from 2 retinas; human INL cells, n = 9 cells from 2 retinas.

(F) Nuclear cross-sectional areas measured from donor and host cells. tdT^+HuNu^+ hRGCs, n = 74 cells from 9 retinas; tdT^-HuNu^- mRGCs, n = 75 cells from 9 retinas; tdT^+ MG:, n = 31 cells from 11 retinas; tdT^-HuNu^- INL mouse neurons, n = 46 cells from 9 retinas; ectopic INL hRGCs, n = 40 nuclei from 11 retinas. Scale bars, 10 μm (A and C) and 5 μm (B). Data are represented as mean ± SD.

markers is essential in xenographic transplantation using human donor cells, and we initially hypothesized that immunofluorescence for human-specific antigens would be useful for unambiguously differentiating donor from host retinal cells. Given the established practice of distinguishing human from rodent cells in xenotransplantation paradigms using species-specific antigen labeling (Ribeiro et al., 2021; Gasparini, et al., 2022), we investigated the MT potential of several human-specific markers. In analyzing retinas from *in vivo* transplantation, antibodies against HuNu consistently labeled tdT$^+$ donor hRGCs, which all exhibited characteristic human nuclear localization of the antigen. However, we were surprised to find that of the tdT$^+$ host MG examined (n = 68 cells from 13 eyes), 92.7% expressed HuNu, which correctly localized to the nucleus, while maintaining a typical mouse nuclear architecture (Figure 5A). In addition, we labeled recipient retinas with monoclonal antibody against Ku80, a human-specific nuclear protein required for non-homologous end joining (Rathmell and Chu, 1994), We found that 15.2% of tdT$^+$ host MG co-stained for Ku80 with nuclear localization (n = 46 cells from 12 eyes, Figure 5B). HuNu and Ku80 expression was not detected elsewhere in the host retina. It is remarkable that, within each tdT$^+$ host MG, HuNu and Ku80 localized to the recipient nuclei, suggesting correct nuclear trafficking of these protein antigens. To assess for cellular fusion, we confirmed that each tdT$^+$ host MG only had one nucleus (Video S3).

Next, we immunolabeled transplanted retinas with antibodies specific to antigens from human mitochondria (hMito) (Swana et al., 1977). We found that 72.7% of tdT$^+$ host MG expressed hMito (n = 11 cells from 3 eyes) as discrete labeling in the perinuclear region and in the glial processes (Figures 5D and 5E), similar to the staining pattern found in the hRGCs in the RGCL (Figures 5D and 5E; Video S4). Taken together, these results imply that donor-derived cytoplasmic, nuclear, and mitochondrial antigens can be transferred to and correctly trafficked within host MG (Figure 5C). It remains unclear whether these observations result from transfer of mRNA and/or protein, or even entire organelles.

DISCUSSION

Maintaining the ability to track and discriminate cells of separate origin is key to unambiguously identifying donor versus host cells for analyses following cellular transplantation. MT confounds accurate cell origin determination by intracellular fluorescent markers and undermines the evaluation of neuronal survival, maturation, and integration in transplantation, transdifferentiation, and neurodevelopmental studies (Boudreau-Pinsonneault and Cayouette, 2018; Blackshaw and Sanes, 2021; Johnson et al., 2023). It was previously unknown whether MT occurs in retinal cell types other than photoreceptors. Here, we provide evidence suggesting that hRGCs can participate in unidirectional heterotopic MT with endogenous mouse MG, and that the cargo includes not only cytoplastic fluorescent proteins but also species-specific antigens that have been used widely to distinguish donor- from host-derived cells. Importantly, we did not identify any instances of MT to recipient RGCs, which fortunately obviates potential confusion regarding donor hRGC engraftment in this particular experimental paradigm. Nonetheless, the demonstration that mouse and human retinal cells can be identified based on nuclear morphology with a straightforward and low-cost approach (DAPI staining) represents an important tool for the transplantation field. Although a primary limitation of RGC transplantation work to date has been suboptimal survival and engraftment of donor neurons (Venugopalan et al., 2016; Oswald et al., 2021; Zhang et al., 2021; Aguzzi et al., 2022; Vrathasha et al., 2022), definitive identification of transplanted RGCs within host retinas will only become more critical as the success of transplantation increases.

It is worth considering an alternative hypothesis that cannot be formally ruled out by the present data. It is conceivable that the tdT$^+$ MG seen in our experiments may have been donor derived, if: a small subpopulation of donor cells (trans)differentiated into an MG phenotype, migrated into the INL, adopted a radial morphology indistinguishable from host MG, received GFP from host-to-donor MT while maintaining tdT expression (or ectopically expressed tdT from the *BRN3B* locus despite adopting an MG fate), altered their nuclear morphology to resemble that of murine retinal cells, and (unlike their donor RGC counterparts) exhibited less than uniform expression of HuNu, Ku80, and hMito. While such successful transplantation-based MG replacement would be remarkable in itself, Occam's razor suggests that mere donor-to-host MT is the more likely explanation for the observations described.

A significant finding from this study is the role of the host microenvironment in simultaneously permitting hRGC integration into the retinal parenchyma and MT to host MG. We have previously demonstrated enhanced hRGC dendrite extension into the IPL following targeted ILM disruption (Zhang et al., 2021; Aguzzi et al., 2022), which correlates with observations made in PR transplantation. Subretinal injection of donor PRs into *Nrl*$^{-/-}$ host retinas in which the OLM is disrupted (Waldron et al., 2018), and in retinas with disrupted tight junctions along the OLM (Stuck et al., 2012), both resulted in increased donor PR integration (West et al., 2008; Pearson et al., 2010;

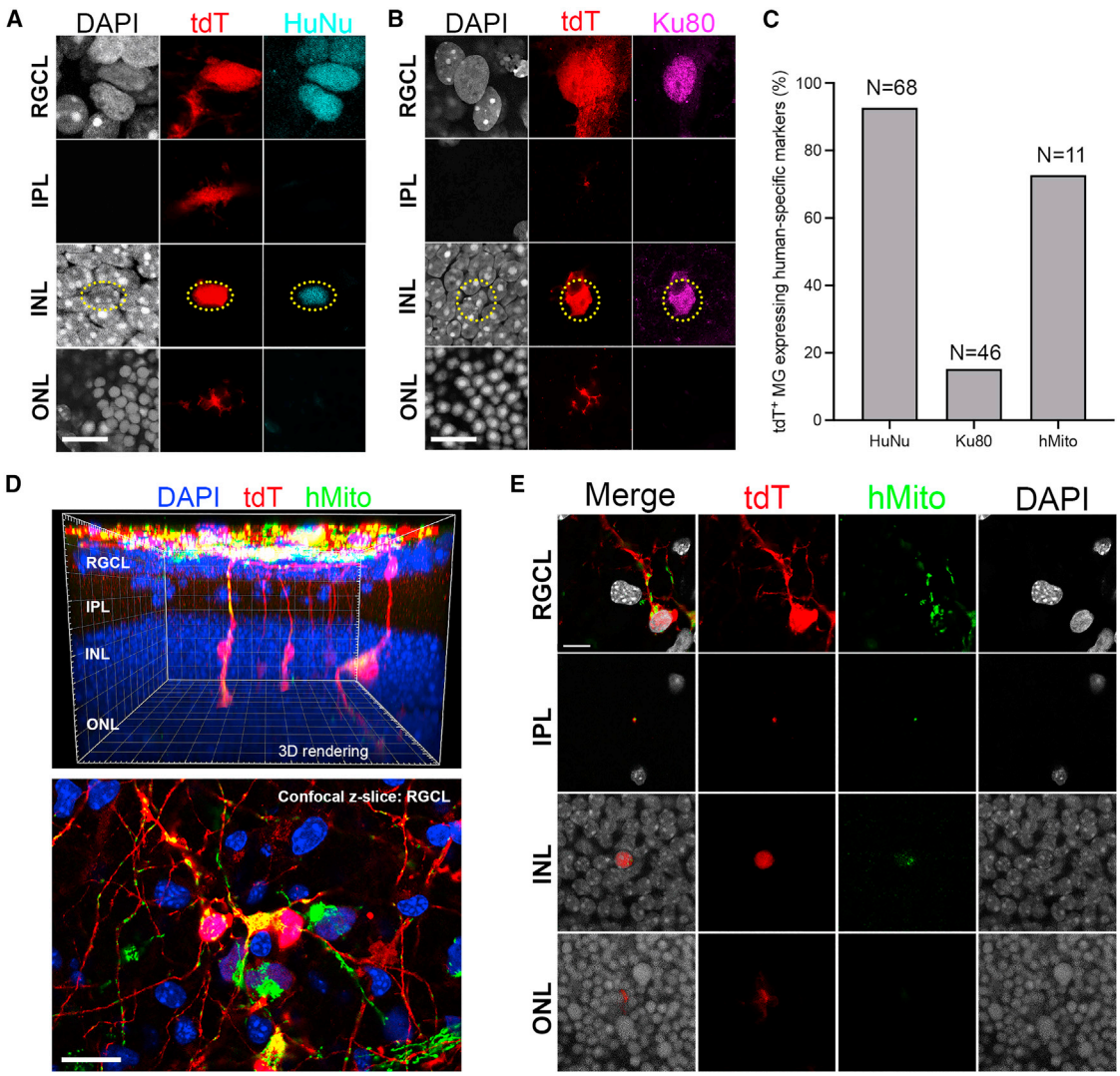

Figure 5. Human-specific donor markers are transferred to host MG *in vivo*

(A) Confocal z slice micrographs of a single tdT$^+$ MG contacting donor hRGCs, labeled with DAPI (gray), tdT (red), and HuNu (cyan). HuNu labeled the euchromatic human nuclei in the RGCL (some of which were tdT$^-$) as well as the heterochromatic MG nucleus in the INL.

(B) Confocal z slice micrographs of a single tdT$^+$ MG contacting a donor hRGC, labeled with DAPI (gray), tdT (red), and Ku80 (magenta). The euchromatic human nucleus in the RGCL as well as the heterochromatic MG nucleus in the INL both expressed Ku80.

(C) Prevalence of human-specific markers localizing within host MG. HuNu, n = 68 MG from 5 retinas; Ku80, n = 46 MG from 12 retinas; hMito, n = 11 MG from 3 retinas).

(D) 3D reconstruction of confocal z stack labeled with tdT (red), hMito (green), and DAPI (blue). Top: profile view of the confocal z stack showing extensive hMito expression near the vitreal surface where donor hRGCs reside; scant hMito labeling was also found deeper in the retina and exclusively in the radial processes of several tdT$^+$ MGs. Bottom: en face view of the RGCL from the same confocal z stack. hMito was confined to tdT$^+$ donor hRGC soma and neurites.

(E) Confocal z slice micrographs of a single tdT$^+$ MG contacting a donor hRGC, labeled with DAPI (gray), tdT (red), and hMito (green). hMito was found in the soma and neurites of a tdT$^+$ hRGC in the RGCL, as well as in the stalk and soma of the tdT$^+$ MG. Scale bars, 10 μm (A, B, and E) and 15 μm (D). Data are represented as mean ± SD.

Barber et al., 2013). The ILM and OLM serve as structural components of the retinal tissue, and their disruption enhances the structural engraftment of donor cells into the neural retina (Zhang and Johnson 2021). But, beyond enabling enhanced donor neuronal engraftment, studying the effects of ILM disruption on hRGC-to-MG MT provided strong evidence that the mechanism of MT in this case is cell contact mediated. The exclusivity of endogenous MG

as the MT recipient is intriguing, perhaps owing to their functional specialization and unique footplates (Tout et al., 1993; Bringmann et al., 2006; Reichenbach and Bringmann, 2013). Our post-transplantation analysis supported this hypothesis, since all tdT$^+$ MG maintained their structural integrity, and the vast majority of them sustained contact with transplanted hRGCs in the host RGCL. Therefore, ILM disruption may augment direct contact between MG endfeet and grafted hRGC neurites or somata. *In vitro* co-culture of MG and hRGCs did not yield MT despite ample contact among the two cell types, suggesting that factors not present in simple 2D dual cell monolayer co-cultures may be required for MT. One factor may relate to MG polarity and maturation within the retina, which is required to develop the canonical endfeet (Wolburg et al., 1991). The specific contact mechanism at the vitreoretinal interface mediating MT between the MG endfeet and hRGC, whether by TNTs or specialized coupling channels, remains to be determined.

Recent discoveries of TNTs facilitating intercellular communication shed light on the mechanism of MT following PR transplantation. TNTs are specialized filopodia connecting neighboring cytoplasms that allow soluble cargo transport between cells (Rustom et al., 2004; He et al., 2011). Identifying evidence of TNT was inherently challenging in our transplant setting due to the dense overlapping neurites elaborated from the donor hRGCs. Nonetheless, our microscopy analyses demonstrated direct contact between MG terminal stalks and hRGCs near the vitreal surface rather than fine connections, although we could not rule out TNTs in the local vicinity. Ongoing work aims to leverage super-resolution and electron microcscopy to evaluate potential intercellular connections between donor and host cells in high detail. Other possible mechanisms underlying MT, including donor-host cell fusion, donor transdifferentiation, and donor-derived EV-mediated transport, are not substantiated by our findings. Syncytia resulting from cell fusion are expected to be multinuclear, which was not observed in our tdT$^+$ MGs. The absence of diploidy may be explained by local merging of plasma membranes of adjacent cells (Perez-Vargas et al., 2014), but this would not explain the exclusion of host material in the hRGCs in contact with the tdT$^+$ MG. Transdifferentiation was unlikely to have occurred since transformed donor cells, while likely to preserve donor-derived tdT expression, would not be expected to express host GFP signals nor to adopt a nuclear morphology so closely characteristic of host retinal cells. Although we did not observe tdT expression in host MG following treatment with hRGC-derived EVs, we cannot definitely rule out an EV-mediated transport mechanism. Inadequate concentrations of EVs or changes in hRGC EV composition following transplantation may have reduced sensitivity of our assay. In addition, our EVs were obtained from hESC cultures in late stages of RGC differentiation. Due to multiple cell types having potential to secrete EVs (Gassama and Faver-eaux, 2021), purification of transplanted hRGC-specific EVs was not feasible.

Central to our determination of MT was the ability to discriminate donor versus host cells, which in xenotransplantation could be sufficiently achieved through parsing human from mouse cells. Microscopic analyses of DAPI stained nuclei reliably revealed distinct patterns in nuclear organization between human and mouse retinal cells. Although human and non-human primate RGCs have been shown to contain nucleoli when stained with cresyl violet or phenylenediamine (Curcio and Allen, 1990; Glovinsky et al., 1993), they are not prominent when stained with DAPI. A common paradigm in nuclear organization is to sequester the transcriptionally repressive domains to the nuclear periphery by tethering to the nuclear membrane, thereby partitioning the euchromatic regions to the nuclear interior accessible to transcriptional machinery (Feodorova et al., 2020). The nuclei in mouse INL and RGCL were characterized by marked clustering of heterochromatic regions, which was not a feature in the DAPI-stained human retinal nuclei, regardless of integration status or derivation from either pluripotent cells or primary human retinal tissue. Chromatin topology modulates retinal development, and differences in the nuclear organization of nocturnal versus diurnal animals may explain why human retinal nuclei lacked these gross morphologic heterochromatic domains (Daghsni and Aldiri, 2021). Critically, our robust demonstration of using intrinsic properties to assess cell identity provides a useful tool for further xenotransplantation studies using human donor cells, particularly since we have now shown that traditional human-specific markers can be trafficked and correctly localized within the host cells.

Finally, the discovery that donor-derived material could be transferred to MG raises the potential for novel therapeutics to repopulate lost RGCs through MG reprogramming. The regenerative potential of MG in zebrafish and avian retinas is increasingly being explored as an avenue to enhance regeneration in the mammalian retina. Viral-based targeting of mammalian MG has long been used to activate their neuroprotective and neurogenic potential (Di Polo et al., 1998; Dalkara et al., 2011; Yao et al., 2016; Hoang et al., 2020; Todd et al., 2022). Fusion between mouse MG and intravitreally transplanted hematopoietic stem and progenitor cells is capable of reprogramming MG into retinal progenitors (Sanges et al., 2016). The resulting fusion events upregulated the Wnt/β-catenin pathway in the hybrid cells, which subsequently differentiated into RGCs, amacrine cells, and photoreceptors (Sanges et al., 2013). Although MT in our context was unlikely to

occur from cell fusion, we speculate that donor hRGCs might be utilized to transfer signals, perhaps those involving the Wnt/β-catenin pathway, into MG to initiate or augment the recipient endogenous repair capacity, if the efficiency of this phenomenon could be dramatically increased. Harnessing discoveries in RGC-MG communication could provide a new avenue toward cell replacement via endogenous cell sources.

Conclusions

Transplantation of hRGCs into mouse retinas following ILM disruption results in transfer of donor material to recipient MG, including fluorescent proteins and nuclear and mitochondrial antigens. This novel form of MT should prompt rigorous evaluation and reporting of MT in intravitreal transplantation studies, and warrants further study to define a full mechanistic characterization of this phenomenon. The transfer of species-specific antigens to host retinal cells suggests that labeling tissues with donor-specific antibodies is, on its own, insufficient to exclude the possibility of artifactual labeling of host cells. The restriction of MT from hRGCs to MG may indicate opportunities to capitalize on the therapeutic potential of MT-mediated MG reprogramming.

EXPERIMENTAL PROCEDURES

Resource availability

Corresponding author

Further information and requests for resources and reagents should be directed to and will be fulfilled by the corresponding author, Thomas V. Johnson (johnson@jhmi.edu).

Materials availability

This study did not generate new unique reagents.

Data and code availability

- All data reported in this paper will be shared by the lead contact upon request.
- This paper does not report original code.
- Any additional information required to reanalyze the data reported in this paper is available from the lead contact upon request.
- Single-cell RNA sequencing data associated with this paper have been uploaded to the Gene Expression Omnibus repository (accession no. GSE242537).

Animals

Adult (age 8–16 weeks) C57BL/6J and C57BL/6-Tg(CAG-EGFP) 10sb/J mice (The Jackson Laboratory, Bar Harbor, ME) were used. C57BL/6J-Lama1^{nmf223}/J mice were a kind gift from the Malia Edwards laboratory (Johns Hopkins). The CAG-EGFP mouse line ubiquitously expressed EGFP by the CAG promoter to provide endogenous fluorescence in almost all tissues, including all retinal cells (Okabe et al., 1997). The Lama1^{nmf223} mouse line harbors an autosomal recessive point mutation at a critical bindings site in *laminin-α1* causing small breaks in the ILM during development (Edwards, et al., 2010; Edwards et al., 2011). Animals were housed in controlled conditions with 12 h light/dark cycle and access to water and food *ad libitum*. Animals of both sexes were used and randomly distributed among experimental groups. All animal protocols adhered to the ARVO Statement for the Use of Animals in Ophthalmic and Vision Research and was approved by Johns Hopkins University Animal Care and Use Committee.

Cell lines and culture

Human H7 and H9 ESCs (WiCell, Madison, WI) carrying *tdTomato* and *CD90.2/Thy1.2* at the endogenous *POU4F2 (BRN3B)* locus (kindly provided by the Don Zack Laboratory, Johns Hopkins) (Sluch et al., 2017) were maintained in mTeSR1 medium (STEMCELL Technologies, Cambridge, MA) on growth factor-reduced Matrigel substrate (Corning, Corning, NY) at 10% CO_2, 5% O_2, and 37°C. Differentiation to RGC fate and immunopurification to >95% tdT$^+$ cells were performed as described previously (Sluch et al., 2017). Cells were counted and cryopreserved at 1 × 10^7 cells/mL in liquid nitrogen until use. MG (human MG cell line Moorefields/Institute of Ophthalmology—Müller 1 [MIO-M1] [Limb et al., 2002], obtained from the UCL Institute of Ophthalmology, London, UK) were used in MG-hRGC co-culture experiments. Co-cultures were established by seeding hRGCs and MG (1:1 ratio, 10^5 cells per well) in a laminin-coated 6-well plate, and incubated in RGC explant medium at 37°C and 5% CO_2 for 5 days. The experimental use of human pluripotent stem cells was approved by Johns Hopkins University Institutional Stem Cell Research Oversight Committee.

Human tissue samples

Postmortem human eyes from a 72-year-old male and an 87-year-old female with no known past ocular history were obtained from the Lions Gift of Sight Eyebank (St Paul, MN,). Freshly enucleated globes were shipped in vials containing saline-moistened gauze on ice and arrived within 24 h of death. Posterior eye cups were fixed by immersion in 4% paraformaldehyde for 24 h and then embedded in OCT and frozen for cryosectioning.

Organotypic mouse and human retinal explant cultures

Organotypic mouse retinal explants were prepared according to established protocols (Johnson et al., 2010; Zhang et al., 2021; Zhang and Johnson, 2022). In brief, animals were euthanized by overdose of intraperitoneal ketamine and xylazine followed by cervical dislocation. Enucleated eyes were rinsed in cold PBS and subsequently dissected to dislodge the neuroretina from the eyecup and the retinal pigmented epithelium. Four relaxing radial incisions were made to create a Maltese cross configuration to facilitate flatmounting on polytetrafluoroethylene organotypic filters (Millipore-Sigma, Burlington, MA). Organotypic retinal explants were cultured with the photoreceptor side against the filter membrane at the fluid/air interface overlying culture medium composed of Neurobasal-A, B27 supplement (2%), N2 supplement (1%), L-glutamine (0.8 mM), penicillin (100 U/mL), and streptomycin (100 μg/mL) (all from Thermo Fisher, Waltham, MA). Explant cultures were incubated in a humidified environment at

37°C and 5% CO_2. Half of the culture medium was exchanged at 1 day *ex vivo* and every 2 days thereafter.

hRGC transplantation and co-culture with retinal explants was performed the day after enzymatic ILM disruption (see below). A 2 μL droplet of cell suspension containing 2 × 10^5 cells was transplanted onto the retinal surface of each explant using a 2 μL pipette.

Enzymatic ILM disruption

Pronase E from *Streptomyces griseus* (Millipore-Sigma) was reconstituted at 0.6 U/mL (for *in vitro* experiments) or 0.08 U/mL (for *in vivo* experiments) in BSS and syringe-filtered before use. A 10 μL pipette was used to dispense 5 μL of Pronase E onto the inner retinal surface of retinal explants. The enzymatic reaction was terminated after 1 h with 300 μL of inhibitor solution (0.15 mM BSA and 0.375 mM Ovomucoid in BSS), followed by a washout with 3 mL of BSS. Treatment solutions were then removed before transferring the culture inserts into a fresh set of 6-well plates with culture medium at 37°C overnight. Pronase E was injected intravitreally into live mice using a transscleral approach with a 33-guage needle for *in vivo* experiments and hRGCs were transplanted 2 weeks later. For treatment of retinal explants with hRGC EVs, concentrated EVs (see below) were applied to the vitreous surface of flatmounted retinas (5 μL) using a 10 μL pipette on a daily basis for 7 days.

In vivo intravitreal RGC transplantation

Recipient animals were anesthetized by intraperitoneal injection of ketamine (50 mg/kg) and xylazine (5 mg/kg). Pupil dilation prior to injection was achieved with 2.5% phenylephrine hydrochloride eye drops (Akorn, Lake Forest). A 33-gauge metal needle (Hamilton, Reno, NV) on a 10 μL Hamilton syringe (Hamilton) was used to puncture the sclera and deliver a transretinal intravitreal injection. Enzyme (2 μL) or hRGCs (3.75 × 10^5 cells) were administered to each eye using a microinjection syringe pump (World Precision Instruments, Sarasota, FL). Animals were sacrificed 2 weeks post-transplantation for evaluation. Histological specimens were included as long as at least one tdT^+ cell was present in the retina.

Immunohistochemistry

Immunohistochemistry was performed on retinal wholemounts according to the methods described previously (Zhang et al., 2021; Zhang and Johnson, 2022). Retinal wholemounts were fixed in 4% PFA at 4°C for 1 h, then washed with 0.1 M PBS for 20 min prior to blocking and permeabilization at room temperature (RT) with 10% normal goat serum (NGS) (Sigma-Aldrich, Milwaukee, WI) and 0.5% Triton X-100 (Sigma-Aldrich) in PBS for 1 h. Tissues were then incubated with primary antibodies diluted in blocking solution (Table S1) for 5 days at 4°C with gentle rocking. Following three 10-min washes in PBS, the samples were immunolabeled with species-specific fluorescently conjugated secondary antibodies diluted 1:1,000 in blocking solution overnight at 4°C in the dark. The tissues were counterstained with DAPI (Sigma-Aldrich) before adding mounting medium (Agilent Technologies, Santa Clara, CA) on glass slides for microscopy.

To obtain cryosections, murine retinal wholemounts were washed in PBS and placed in 25% sucrose in PBS for 24 h before freezing in optimal cutting temperature embedding compound (Sakura Finetek, Torrance, CA) on dry ice. Frozen tissue blocks of mouse retinas or human posterior eye cups were sectioned at 16 μm using a Leica cryostat (Leica Biosystems, Buffalo Grove, IL). Cryosections were washed with PBS for 5 min followed by blocking in 10% NGS for 1 h, then incubated in primary antibody (Table S1) overnight at 4°C. The sections were then washed with PBS and incubated with corresponding secondary polyclonal goat antibody for 1 h at RT. Slides were counterstained with DAPI (Sigma-Aldrich) before coverslipping over mounting medium (Agilent Technologies).

Confocal microscopy

Fluorescently labeled retinal flatmounts with the photoreceptor side down were visualized and imaged with the ILM en face using a Zeiss LSM 880 confocal microscope equipped with Zen software (Carl Zeiss, Peabody, MA) (Zhang and Johnson, 2022). High-resolution images (2,048 × 2,048 pixels) were acquired using identical fluorescent settings with Zeiss 63×/1.4 PlanApo oil immersion or 40×/1.2 C-Apo water immersion objectives. The pinhole was set to 1 Airy unit and confocal slices were numbered to optimize the axial resolution for the particular objective being used. 3D renderings of confocal z stacks were generated using Imaris (Oxford Instruments, Oxon, UK). Investigators were masked to treatment groups to ensure unbiased selection of fields for imaging. Unmasking occurred only after microscopy and image analysis.

EV isolation and analyses

EVs were isolated from serum-free culture-conditioned medium (CCM) from hESC to RGC differentiations at day 35–40, when RGC differentiation is maximal, using ultracentrifugation as described previously (Thery et al., 2006). An initial 500 mL of CCM was concentrated approximately 10× by tangential flow filtration using a membrane with 100 kDa molecular weight cutoff (Sartorius, Goettingen, Germany). Concentrated CCM was centrifuged at 1,000 × *g* for 5 min to remove cell debris. The supernatant was transferred to 10 mL polycarbonate ultracentrifuge tubes (Beckman Coulter, Brea, CA) and ultracentrifuged (100,000 × *g* for 70 min) at 4°C using a TI-50 fixed-angle rotor (Beckman Coulter). The resulting supernatant was discarded and the pellets containing EVs were resuspended in UltraPure water (Thermo Fisher Scientific) and stored at −80°C.

Microfluidic resistive pulse sensing was used to determine the EV particle concentration and size distribution (Fraikin et al., 2011). All samples were measured with a Spectradyne nCS1 instrument (Spectradyne, Torrance, CA) equipped with TS-400 or -900 polydimethylsiloxane cartridges. Calibration was performed using 150 and 505 nm diameter polystyrene standard beads at a concentration of 2 × 10^9 beads/mL. Sample volumes of 5 μL at 10^9–10^{10} particles/mL of PBS were loaded into the cartridges. A minimum of 10,000 particle transition events were counted per analysis. Fractional size distributions were also measured by single-particle interferometric reflectance imaging of EVs captured on the surface of tetraspanin-specific ExoView chips (NanoView Biosciences, Brighton, MA).

(1) Common EV biomarkers (CD9, CD63, and CD81) (Kowal et al., 2016) were characterized using ExoView Tetraspanin

Kits on the ExoView R100 imaging platform (NanoView Biosciences) and subsequently verified by western blot assays under both reducing and non-reducing conditions. Antibody against the mitochondrial membrane protein VDAC-1 (Santa Cruz Biotechnologies) was used to check for mitochondrial membrane contaminants. Protein concentrations in all samples were verified with the Pierce BCA Protein Assay Kit (Thermo Fisher Scientific).

(2) A total of 10 μL freshly thawed EV aliquots were adsorbed to glow-discharged carbon-coated 400 mesh copper grids by floatation for 2 min. Grids were quickly blotted then rinsed in 3 drops of 1× Tris-buffered saline. Grids were negatively stained in two consecutive drops of 1% uranyl acetate with tylose (1% UAT in dH_2O, double filtered through a 0.22 μm filter), blotted, then quickly aspirated to get a thin layer of stain covering the sample. Grids were imaged on a Phillips CM-120 TEM operating at 80 kV with an 8-megapixel AMT XR80 CCD.

Total RNA was extracted from sorted retinal cells or EVs using TRIzol (Thermo Fisher Scientific) according to manufacturer's instructions. RNA quantity was measured using a NanoDrop 2000 UV-vis spectrophotometer (Thermo Fisher Scientific) and integrity confirmed by 1% agarose gel electrophoresis. RNA from each sample (500 ng) was reverse transcribed into complementary DNA (cDNA) using the High-Capacity cDNA Reverse Transcription Kit (Thermo Fisher Scientific) in a 20 μL reaction volume. The thermocycler was programmed to run for 10 min at 25°C, then 120 min at 37°C, followed by 5 min at 85°C. The amplified cDNA templates were stored at −20°C until use. qRT-PCR was performed on a CFX384 Touch Real-Time PCR Detection system with SsoAdvanced Universal SYBR Green SuperMix (both from Bio-Rad, Hercules, CA). Synthesized cDNA was diluted to a 1:5 working stock. Each reaction contained 1 μL of the diluted cDNA template, 2.5 μL of SYBR Green SuperMix, 0.05 μL of primer set (100 μM stock), and 4 μL of nuclease-free water, for a total volume of 5 μL. A separate no template control was included in the reaction set. All target genes and oligonucleotide sequences (Table S1) were designed and verified using Primer-BLAST (www.ncbi.nlm.nih.gov/tools/primer-blast/). All primer sets were validated by standard curves and melt curve analyses. The qRT-PCR conditions were set as follows: 95°C for 30 s, followed by 40 cycles of 95°C for 15 s, then 60°C for 30 s. The relative gene expression (normalized to the mean expression in hRGCs) was calculated and graphed using Prism 9 (GraphPad Software, San Diego, CA). Three biological replicates of three technical triplicates were analyzed per primer set.

Single-cell RNA sequencing library preparation and analysis

hESC-derived RGCs were purified as described above. The purified RGCs were subsequently used for single-cell RNA sequencing library preparation using Drop-seq. The resulting library was sequenced on a Novaseq 6000 instrument. The sequencing reads were aligned to the GRCh38 reference genome and subsequently processed to generate a gene expression matrix using the Drop-seq data processing pipeline. Following this, the cells were normalized, scaled, and clustered using the Seurat package with default parameters. To predict the cell identities, a human fetal retinal single-cell RNA sequencing was utilized as a reference dataset (Hu et al., 2019). By comparing our dataset to the human fetal dataset using Seurat label transfer, our cells were assigned identities based on their highest similarity to the human fetal cells.

Quantification and statistical analyses

All imaging and data qualification was performed by investigators who were masked to treatment groups; unmasking was performed only after raw data were generated. Results are reported as mean ± standard deviation unless otherwise stated. For *ex vivo* and *in vivo* studies, each retina was considered a single experimental unit. Each experiment was performed at least twice. Data were analyzed using SPSS (v.25, IBM, Armonk, NY) and plotted using Prism (v.8.0, GraphPad Software). Significance level was defined as $p < 0.05$. Experimental schematics in Figures 1A, 1F, 3E, and 3H were created using Biorender.com.

SUPPLEMENTAL INFORMATION

Supplemental information can be found online at https://doi.org/10.1016/j.stemcr.2023.09.005.

ACKNOWLEDGMENTS

Funding for this work was provided by The National Eye Institute (NIH, Bethesda, MD; K08EY031801, R21EY034332, and P30EY 001765), Research to Prevent Blindness (New York, NY; Clinician Scientist Development Award (to T.V.J.) and unrestricted funding to the Wilmer Eye Institute), the BrightFocus Foundation (Clarksburg, MD; G2002005S), the Zenkel Family Foundation (New York, NY), and the Shelley & Alan Holt Rising Professorship in Ophthalmology. We thank Astrid Limb (University College London) for providing the MIO-M1 cell line used in in this work.

AUTHOR CONTRIBUTIONS

Conceptualization, T.V.J.; methodology, K.Y.Z., M.E.P., D.J.Z., and T.V.J.; formal analysis, K.Y.Z. and T.V.J.; investigation, K.Y.Z., A.N., E.A.A., S.M., N.C., B.S., S.M., and T.V.J.; data curation, K.Y.Z. and T.V.J.; writing – original draft, K.Y.Z. and T.V.J.; writing – review & editing, K.Y.Z., A.N., E.A.A., S.M., N.C., M.E.P., M.E.E., H.A.Q., and T.V.J.; visualization, K.Y.Z. and T.V.J.; validation, M.E.P.; resources, M.E.P., M.E.E., H.A.Q., and D.J.Z.; supervision, D.J.Z. and T.V.J; project administration, D.J.Z. and T.V.J; funding acquisition, D.J.Z. and T.V.J.

DECLARATION OF INTERESTS

The authors declare no competing interests.

Received: March 20, 2023
Revised: September 7, 2023
Accepted: September 8, 2023
Published: October 5, 2023

REFERENCES

Aguzzi, E.A., Zhang, K.Y., Nagalingam, A., Quillen, S., Hariharakumar, S., Chetla, N., Madhoun, S., Edwards, M.M., Quigley, H.A.,

Zack, D.J., and Johnson, T.V. (2022). Internal limiting membrane disruption facilitates engraftment of transplanted human stem cell derived retinal ganglion cells. Preprint at bioRxiv. https://doi.org/10.1101/2022.12.13.519327.

Arab, T., Mallick, E.R., Huang, Y., Dong, L., Liao, Z., Zhao, Z., Gololobova, O., Smith, B., Haughey, N.J., Pienta, K.J., et al. (2021). Characterization of extracellular vesicles and synthetic nanoparticles with four orthogonal single-particle analysis platforms. J. Extracell. Vesicles *10*, e12079.

Barber, A.C., Hippert, C., Duran, Y., West, E.L., Bainbridge, J.W.B., Warre-Cornish, K., Luhmann, U.F.O., Lakowski, J., Sowden, J.C., Ali, R.R., and Pearson, R.A. (2013). Repair of the degenerate retina by photoreceptor transplantation. Proc. Natl. Acad. Sci. USA *110*, 354–359.

Blackshaw, S., and Sanes, J.R. (2021). Turning lead into gold: reprogramming retinal cells to cure blindness. J. Clin. Invest. *131*, e146134.

Boudreau-Pinsonneault, C., and Cayouette, M. (2018). Cell lineage tracing in the retina: Could material transfer distort conclusions? Dev. Dynam. *247*, 10–17.

Bringmann, A., Pannicke, T., Grosche, J., Francke, M., Wiedemann, P., Skatchkov, S.N., Osborne, N.N., and Reichenbach, A. (2006). Muller cells in the healthy and diseased retina. Prog. Retin. Eye Res. *25*, 397–424.

Budnik, V., Ruiz-Cañada, C., and Wendler, F. (2016). Extracellular vesicles round off communication in the nervous system. Nat. Rev. Neurosci. *17*, 160–172.

Curcio, C.A., and Allen, K.A. (1990). Topography of ganglion cells in human retina. J. Comp. Neurol. *300*, 5–25.

Daghsni, M., and Aldiri, I. (2021). Building a Mammalian Retina: An Eye on Chromatin Structure. Front. Genet. *12*, 775205.

Dalkara, D., Kolstad, K.D., Guerin, K.I., Hoffmann, N.V., Visel, M., Klimczak, R.R., Schaffer, D.V., and Flannery, J.G. (2011). AAV mediated GDNF secretion from retinal glia slows down retinal degeneration in a rat model of retinitis pigmentosa. Mol. Ther. *19*, 1602–1608.

Decembrini, S., Martin, C., Sennlaub, F., Chemtob, S., Biel, M., Samardzija, M., Moulin, A., Behar-Cohen, F., and Arsenijevic, Y. (2017). Cone Genesis Tracing by the Chrnb4-EGFP Mouse Line: Evidences of Cellular Material Fusion after Cone Precursor Transplantation. Mol. Ther. *25*, 634–653.

Di Polo, A., Aigner, L.J., Dunn, R.J., Bray, G.M., and Aguayo, A.J. (1998). Prolonged delivery of brain-derived neurotrophic factor by adenovirus-infected Muller cells temporarily rescues injured retinal ganglion cells. Proc. Natl. Acad. Sci. USA *95*, 3978–3983.

Edwards, M.M., Mammadova-Bach, E., Alpy, F., Klein, A., Hicks, W.L., Roux, M., Simon-Assmann, P., Smith, R.S., Orend, G., Wu, J., et al. (2010). Mutations in Lama1 disrupt retinal vascular development and inner limiting membrane formation. J. Biol. Chem. *285*, 7697–7711.

Edwards, M.M., McLeod, D.S., Grebe, R., Heng, C., Lefebvre, O., and Lutty, G.A. (2011). Lama1 mutations lead to vitreoretinal blood vessel formation, persistence of fetal vasculature, and epiretinal membrane formation in mice. BMC Dev. Biol. *11*, 60.

Feodorova, Y., Falk, M., Mirny, L.A., and Solovei, I. (2020). Viewing Nuclear Architecture through the Eyes of Nocturnal Mammals. Trends Cell Biol. *30*, 276–289.

Fraikin, J.L., Teesalu, T., McKenney, C.M., Ruoslahti, E., and Cleland, A.N. (2011). A high-throughput label-free nanoparticle analyser. Nat. Nanotechnol. *6*, 308–313.

Gasparini, S.J., Tessmer, K., Reh, M., Wieneke, S., Carido, M., Völkner, M., Borsch, O., Swiersy, A., Zuzic, M., Goureau, O., et al. (2022). Transplanted human cones incorporate into the retina and function in a murine cone degeneration model. J. Clin. Invest. *132*, e154619.

Gassama, Y., and Favereaux, A. (2021). Emerging Roles of Extracellular Vesicles in the Central Nervous System: Physiology, Pathology, and Therapeutic Perspectives. Front. Cell. Neurosci. *15*, 626043.

Generous, A.R., Harrison, O.J., Troyanovsky, R.B., Mateo, M., Navaratnarajah, C.K., Donohue, R.C., Pfaller, C.K., Alekhina, O., Sergeeva, A.P., Indra, I., et al. (2019). Trans-endocytosis elicited by nectins transfers cytoplasmic cargo, including infectious material, between cells. J. Cell Sci. *132*, jcs235507.

Glovinsky, Y., Quigley, H.A., and Pease, M.E. (1993). Foveal Ganglion-Cell Loss Is Size Dependent in Experimental Glaucoma. Invest. Ophthalmol. Vis. Sci. *34*, 395–400.

He, K., Shi, X., Zhang, X., Dang, S., Ma, X., Liu, F., Xu, M., Lv, Z., Han, D., Fang, X., and Zhang, Y. (2011). Long-distance intercellular connectivity between cardiomyocytes and cardiofibroblasts mediated by membrane nanotubes. Cardiovasc. Res. *92*, 39–47.

Heisterkamp, P., Borsch, O., Lezama, N.D., Gasparini, S., Fathima, A., Carvalho, L.S., Wagner, F., Karl, M.O., Schlierf, M., and Ader, M. (2022). Evidence for endogenous exchange of cytoplasmic material between a subset of cone and rod photoreceptors within the adult mammalian retina via direct cell-cell connections. Exp. Eye Res. *219*, 109033.

Hoang, T., Wang, J., Boyd, P., Wang, F., Santiago, C., Jiang, L., Yoo, S., Lahne, M., Todd, L.J., Jia, M., et al. (2020). Gene regulatory networks controlling vertebrate retinal regeneration. Science *370*, eabb8598.

Hu, Y., Wang, X., Hu, B., Mao, Y., Chen, Y., Yan, L., Yong, J., Dong, J., Wei, Y., Wang, W., et al. (2019). Dissecting the transcriptome landscape of the human fetal neural retina and retinal pigment epithelium by single-cell RNA-seq analysis. PLoS Biol. *17*, e3000365.

Jeon, C.J., Strettoi, E., and Masland, R.H. (1998). The major cell populations of the mouse retina. J. Neurosci. *18*, 8936–8946.

Johnson, T.V., Bull, N.D., Hunt, D.P., Marina, N., Tomarev, S.I., and Martin, K.R. (2010). Neuroprotective effects of intravitreal mesenchymal stem cell transplantation in experimental glaucoma. Invest. Ophthalmol. Vis. Sci. *51*, 2051–2059.

Johnson, T.V., Calkins, D.J., Fortune, B., Goldberg, J.L., La Torre, A., Lamba, D.A., Meyer, J.S., Reh, T.A., Wallace, V.A., Zack, D.J., and Baranov, P. (2023). The importance of unambiguous cell origin determination in neuronal repopulation studies. iScience *26*, 106361.

Kalargyrou, A.A., Basche, M., Hare, A., West, E.L., Smith, A.J., Ali, R.R., and Pearson, R.A. (2021). Nanotube-like processes facilitate material transfer between photoreceptors. EMBO Rep. *22*, e53732.

Kowal, J., Arras, G., Colombo, M., Jouve, M., Morath, J.P., Primdal-Bengtson, B., Dingli, F., Loew, D., Tkach, M., and Théry, C. (2016). Proteomic comparison defines novel markers to characterize heterogeneous populations of extracellular vesicle subtypes. Proc. Natl. Acad. Sci. USA *113*, E968–E977.

Limb, G.A., Salt, T.E., Munro, P.M.G., Moss, S.E., and Khaw, P.T. (2002). In vitro characterization of a spontaneously immortalized human Muller cell line (MIO-M1). Invest. Ophthalmol. Vis. Sci. *43*, 864–869.

MacLaren, R.E., Pearson, R.A., MacNeil, A., Douglas, R.H., Salt, T.E., Akimoto, M., Swaroop, A., Sowden, J.C., and Ali, R.R. (2006). Retinal repair by transplantation of photoreceptor precursors. Nature *444*, 203–207.

Manders, E.M., Stap, J., Brakenhoff, G.J., van Driel, R., and Aten, J.A. (1992). Dynamics of three-dimensional replication patterns during the S-phase, analysed by double labelling of DNA and confocal microscopy. J. Cell Sci. *103* (Pt 3), 857–862.

Okabe, M., Ikawa, M., Kominami, K., Nakanishi, T., and Nishimune, Y. (1997). Green mice' as a source of ubiquitous green cells. FEBS Lett. *407*, 313–319.

Ortin-Martinez, A., Tsai, E.L.S., Nickerson, P.E., Bergeret, M., Lu, Y., Smiley, S., Comanita, L., and Wallace, V.A. (2017). A Reinterpretation of Cell Transplantation: GFP Transfer From Donor to Host Photoreceptors. Stem Cell. *35*, 932–939.

Ortin-Martinez, A., Yan, N.E., Tsai, E.L.S., Comanita, L., Gurdita, A., Tachibana, N., Liu, Z.C., Lu, S., Dolati, P., Pokrajac, N.T., et al. (2021). Photoreceptor nanotubes mediate the in vivo exchange of intracellular material. EMBO J. *40*, e107264.

Oswald, J., Kegeles, E., Minelli, T., Volchkov, P., and Baranov, P. (2021). Transplantation of miPSC/mESC-derived retinal ganglion cells into healthy and glaucomatous retinas. Mol. Ther. Methods Clin. Dev. *21*, 180–198.

Pearson, R.A., Barber, A.C., Rizzi, M., Hippert, C., Xue, T., West, E.L., Duran, Y., Smith, A.J., Chuang, J.Z., Azam, S.A., et al. (2012). Restoration of vision after transplantation of photoreceptors. Nature *485*, 99–103.

Pearson, R.A., Barber, A.C., West, E.L., MacLaren, R.E., Duran, Y., Bainbridge, J.W., Sowden, J.C., and Ali, R.R. (2010). Targeted Disruption of Outer Limiting Membrane Junctional Proteins (Crb1 and ZO-1) Increases Integration of Transplanted Photoreceptor Precursors Into the Adult Wild-Type and Degenerating Retina. Cell Transplant. *19*, 487–503.

Pearson, R.A., Gonzalez-Cordero, A., West, E.L., Ribeiro, J.R., Aghaizu, N., Goh, D., Sampson, R.D., Georgiadis, A., Waldron, P.V., Duran, Y., et al. (2016). Donor and host photoreceptors engage in material transfer following transplantation of post-mitotic photoreceptor precursors. Nat. Commun. *7*, 13029.

Pérez-Vargas, J., Krey, T., Valansi, C., Avinoam, O., Haouz, A., Jamin, M., Raveh-Barak, H., Podbilewicz, B., and Rey, F.A. (2014). Structural basis of eukaryotic cell-cell fusion. Cell *157*, 407–419.

Rathmell, W.K., and Chu, G. (1994). Involvement of the Ku autoantigen in the cellular response to DNA double-strand breaks. Proc. Natl. Acad. Sci. USA *91*, 7623–7627.

Reichenbach, A., and Bringmann, A. (2013). New functions of Muller cells. Glia *61*, 651–678.

Reichenbach, A., and Bringmann, A. (2020). Glia of the human retina. Glia *68*, 768–796.

Ribeiro, J., Procyk, C.A., West, E.L., O'Hara-Wright, M., Martins, M.F., Khorasani, M.M., Hare, A., Basche, M., Fernando, M., Goh, D., et al. (2021). Restoration of visual function in advanced disease after transplantation of purified human pluripotent stem cell-derived cone photoreceptors. Cell Rep. *35*, 109022.

Rustom, A., Saffrich, R., Markovic, I., Walther, P., and Gerdes, H.H. (2004). Nanotubular highways for intercellular organelle transport. Science *303*, 1007–1010.

Sakami, S., Imanishi, Y., and Palczewski, K. (2019). Muller glia phagocytose dead photoreceptor cells in a mouse model of retinal degenerative disease. Faseb. J. *33*, 3680–3692.

Sanges, D., Romo, N., Simonte, G., Di Vicino, U., Tahoces, A.D., Fernández, E., and Cosma, M.P. (2013). Wnt/beta-catenin signaling triggers neuron reprogramming and regeneration in the mouse retina. Cell Rep. *4*, 271–286.

Sanges, D., Simonte, G., Di Vicino, U., Romo, N., Pinilla, I., Nicolás, M., and Cosma, M.P. (2016). Reprogramming Muller glia via in vivo cell fusion regenerates murine photoreceptors. J. Clin. Invest. *126*, 3104–3116.

Santos-Ferreira, T., Llonch, S., Borsch, O., Postel, K., Haas, J., and Ader, M. (2016). Retinal transplantation of photoreceptors results in donor-host cytoplasmic exchange. Nat. Commun. *7*, 13028.

Singh, M.S., Balmer, J., Barnard, A.R., Aslam, S.A., Moralli, D., Green, C.M., Barnea-Cramer, A., Duncan, I., and MacLaren, R.E. (2016). Transplanted photoreceptor precursors transfer proteins to host photoreceptors by a mechanism of cytoplasmic fusion. Nat. Commun. *7*, 13537.

Singh, M.S., Charbel Issa, P., Butler, R., Martin, C., Lipinski, D.M., Sekaran, S., Barnard, A.R., and MacLaren, R.E. (2013). Reversal of end-stage retinal degeneration and restoration of visual function by photoreceptor transplantation. Proc. Natl. Acad. Sci. USA *110*, 1101–1106.

Singh, M.S., Park, S.S., Albini, T.A., Canto-Soler, M.V., Klassen, H., MacLaren, R.E., Takahashi, M., Nagiel, A., Schwartz, S.D., and Bharti, K. (2020). Retinal stem cell transplantation: Balancing safety and potential. Prog. Retin. Eye Res. *75*, 100779.

Sluch, V.M., Chamling, X., Liu, M.M., Berlinicke, C.A., Cheng, J., Mitchell, K.L., Welsbie, D.S., and Zack, D.J. (2017). Enhanced Stem Cell Differentiation and Immunopurification of Genome Engineered Human Retinal Ganglion Cells. Stem Cells Transl. Med. *6*, 1972–1986.

Stuck, M.W., Conley, S.M., and Naash, M.I. (2012). Defects in the outer limiting membrane are associated with rosette development in the Nrl-/- retina. PLoS One *7*, e32484.

Swana, G.T., Swana, M.R., Bottazzo, G.F., and Doniach, D. (1977). A human-specific mitochondrial antibody its importance in the identification of organ-specific reactions. Clin. Exp. Immunol. *28*, 517–525.

Tham, Y.C., Li, X., Wong, T.Y., Quigley, H.A., Aung, T., and Cheng, C.Y. (2014). Global Prevalence of Glaucoma and Projections of Glaucoma Burden through 2040 A Systematic Review and Meta-Analysis. Ophthalmology *121*, 2081–2090.

Thery, C., Amigorena, S., Raposo, G., and Clayton, A. (2006). Isolation and characterization of exosomes from cell culture supernatants and biological fluids. Curr. Protoc. Cell Biol. **Chapter** *3*. Unit 3 22.

Todd, L., Jenkins, W., Finkbeiner, C., Hooper, M.J., Donaldson, P.C., Pavlou, M., Wohlschlegel, J., Ingram, N., Rieke, F., Reh, T.A., and Mu, X. (2022). Reprogramming Muller glia to regenerate ganglion-like cells in adult mouse retina with developmental transcription factors. Sci. Adv. *8*, eabq7219.

Tout, S., Chan-Ling, T., Holländer, H., and Stone, J. (1993). The role of Muller cells in the formation of the blood-retinal barrier. Neuroscience *55*, 291–301.

Tucker, B.A., Park, I.H., Qi, S.D., Klassen, H.J., Jiang, C., Yao, J., Redenti, S., Daley, G.Q., and Young, M.J. (2011). Transplantation of adult mouse iPS cell-derived photoreceptor precursors restores retinal structure and function in degenerative mice. PLoS One *6*, e18992.

Valiunas, V., Polosina, Y.Y., Miller, H., Potapova, I.A., Valiuniene, L., Doronin, S., Mathias, R.T., Robinson, R.B., Rosen, M.R., Cohen, I.S., and Brink, P.R. (2005). Connexin-specific cell-to-cell transfer of short interfering RNA by gap junctions. J. Physiol. *568*, 459–468.

Venugopalan, P., Wang, Y., Nguyen, T., Huang, A., Muller, K.J., and Goldberg, J.L. (2016). Transplanted neurons integrate into adult retinas and respond to light. Nat. Commun. *7*, 10472.

Vrathasha, V., Nikonov, S., Bell, B.A., He, J., Bungatavula, Y., Uyhazi, K.E., and Murthy Chavali, V.R. (2022). Transplanted human induced pluripotent stem cells-derived retinal ganglion cells embed within mouse retinas and are electrophysiologically functional. iScience *25*, 105308.

Waldron, P.V., Di Marco, F., Kruczek, K., Ribeiro, J., Graca, A.B., Hippert, C., Aghaizu, N.D., Kalargyrou, A.A., Barber, A.C., Grimaldi, G., et al. (2018). Transplanted Donor- or Stem Cell-Derived Cone Photoreceptors Can Both Integrate and Undergo Material Transfer in an Environment-Dependent Manner. Stem Cell Rep. *10*, 406–421.

Welsbie, D.S., Yang, Z.Y., Ge, Y., Mitchell, K.L., Zhou, X.R., Berlinicke, C.A., Hackler, L., Fuller, J., Fu, J., Han, B., et al. (2013). Functional Genomic Screening Identifies Dual Leucine Zipper Kinase as a Key Mediator of Retinal Ganglion Cell Death. Neurotherapeutics *10*, 549–550.

West, E.L., Pearson, R.A., Tschernutter, M., Sowden, J.C., MacLaren, R.E., and Ali, R.R. (2008). Pharmacological disruption of the outer limiting membrane leads to increased retinal integration of transplanted photoreceptor precursors. Exp. Eye Res. *86*, 601–611.

Williams, P.R., Benowitz, L.I., Goldberg, J.L., and He, Z. (2020). Axon Regeneration in the Mammalian Optic Nerve. Annu. Rev. Vis. Sci. *6*, 195–213.

Wolburg, H., Willbold, E., and Layer, P.G. (1991). Muller glia endfeet, a basal lamina and the polarity of retinal layers form properly in vitro only in the presence of marginal pigmented epithelium. Cell Tissue Res. *264*, 437–451.

Yamashita, Y.M., Inaba, M., and Buszczak, M. (2018). Specialized Intercellular Communications via Cytonemes and Nanotubes. Annu. Rev. Cell Dev. Biol. *34*, 59–84.

Yao, K., Qiu, S., Tian, L., Snider, W.D., Flannery, J.G., Schaffer, D.V., and Chen, B. (2016). Wnt Regulates Proliferation and Neurogenic Potential of Muller Glial Cells via a Lin28/let-7 miRNA-Dependent Pathway in Adult Mammalian Retinas. Cell Rep. *17*, 165–178.

Zhang, K.Y., and Johnson, T.V. (2021). The internal limiting membrane: Roles in retinal development and implications for emerging ocular therapies. Exp. Eye Res. *206*, 108545.

Zhang, K.Y., and Johnson, T.V. (2022). Analyses of transplanted human retinal ganglion cell morphology and localization in murine organotypic retinal explant culture. STAR Protoc. *3*, 101328.

Zhang, K.Y., Tuffy, C., Mertz, J.L., Quillen, S., Wechsler, L., Quigley, H.A., Zack, D.J., and Johnson, T.V. (2021). Role of the Internal Limiting Membrane in Structural Engraftment and Topographic Spacing of Transplanted Human Stem Cell-Derived Retinal Ganglion Cells. Stem Cell Rep. *16*, 149–167.